

Article

Pleistocene Calcareous Nannofossil Biostratigraphy and Gephyrocapsid Occurrence in Site U1431D, IODP 349, South China Sea

Jose Dominick S. Guballa ^{*,†} and Alyssa M. Peleo-Alampay

Nannoworks Laboratory, National Institute of Geological Sciences, College of Science, University of the Philippines, Diliman, Quezon City 1101, Philippines; ampeleoalampay@up.edu.ph

* Correspondence: doms.guballa@mail.utoronto.ca; Tel.: +1-28-9707-5905

† Current address: Department of Earth Sciences, University of Toronto, 22 Russell Street, Toronto, ON M5S 3B1, Canada.

Received: 25 August 2020; Accepted: 23 September 2020; Published: 28 September 2020



Abstract: We reinvestigated the Pleistocene calcareous nannofossil biostratigraphy of Site U1431D (International Ocean Discovery Program (IODP) Expedition 349) in the South China Sea (SCS). Twelve calcareous nannofossil Pleistocene datums are identified in the site. The analysis confirms that the last occurrence (LO) of *Calcidiscus macintyreii* is below the first occurrence (FO) of large *Gephyrocapsa* spp. (>5.5 μm). The FO of medium *Gephyrocapsa* spp. (4–5.5 μm) is also identified in the samples through morphometric measurements, which was unreported in shipboard results. Magnetobiochronologic calibrations of the numerical ages of LO of *Pseudoemiliana lacunosa* and FO of *Emiliana huxleyi* are underestimated and need reassessment. Other potential markers such as a morphological turnover of circular to elliptical variants of *Pseudoemiliana lacunosa* and a small *Gephyrocapsa* acme almost synchronous with the FO of *Emiliana huxleyi* may offer biostratigraphic significance in the SCS. The morphologic changes in *Gephyrocapsa* coccoliths are also examined for the first time in Site U1431D. Placolith length and bridge angle changes are comparable with other ocean basins, suggesting that morphologic changes are most likely evolutionary novelties rather than being caused by local climate anomalies.

Keywords: calcareous nannofossils; South China Sea; Pleistocene; International Ocean Discovery Program; Site U1431; *Gephyrocapsa*

1. Introduction

The Pleistocene is characterized by worldwide sea level lows and highs due to increased amplitudes of glacial and interglacial episodes, respectively [1–3]. Ice volume fluctuations are well represented in deep sea sedimentary sequences by variations in proxies such as sediment properties, fossil assemblages, and/or isotope concentrations. The basis for proxy correlations is a precise and robust chronology constructed from natural cycles of sediment physical properties, radiometric ages, magnetic reversals, and/or biostratigraphic data. An accurate age model is important because major climatic shifts in the Pleistocene occurred within a few hundred thousand years, as exemplified by glacial–interglacial amplitude variations in $\delta^{18}\text{O}$ records [2]. Furthermore, several periods in the Pleistocene are thought to be analogs to the modern-day climate, such as Marine Isotope Stage (MIS) 11 [4,5] and may contribute to a further understanding of past and future climate change dynamics. These climatic events can be put into geologic context through relative dating by using calcareous nannofossils.

Calcareous nannofossils are mostly made up of remains of marine, unicellular phytoplankton known as coccolithophores. Coccolithophores produce a robust, calcium carbonate exoskeleton called the coccosphere. The coccosphere disintegrates into its coccoliths (individual calcite plates)

upon death and is incorporated in fecal pellets and/or marine snow, thus dominating the carbonate fraction of deep-sea pelagic sediments. Calcareous nannofossils are utilized in sediment core studies because of their widespread geographic occurrence and stratigraphic significance. They underwent extinction and speciation events (datums) since the Triassic period, defining brief spans of geologic time [6]. The calibration of nannofossil datums through astronomical tuning and cyclostratigraphy has been substantial in creating a robust time scale for the Pleistocene [7–9]. Star-shaped discoasters are mainly used in subdividing the Early Pleistocene [7,10–14]. Gephyrocapsids are also major components of Pleistocene calcareous nannofossil assemblages [15–22]. Gephyrocapsids have been extensively studied because of complex morphological changes, which have been utilized to subdivide the Pleistocene [7,21–24]. However, semi-enclosed marginal seas may have different oceanographic parameters, resulting to a different calcareous nannofossil assemblage. It is therefore important to study the calcareous nannofossil biostratigraphy of marginal seas to verify if standard nannofossil zonations apply to these areas.

The South China Sea (SCS) is the largest marginal sea in the western Pacific area and has been subject to multiple paleoceanographic [25–30] and sedimentological studies [31–34]. The SCS is characterized by better carbonate preservation compared to other western Pacific marginal basins, providing a valuable sediment archive for East Asian Monsoon System (EAMS) variations since the Miocene [35]. Calcareous nannoplankton in surface sediments [36–39] have also been studied in the northern, western, and eastern SCS. Despite increasing scientific attention on the SCS, calcareous nannofossil biostratigraphic studies of Pleistocene deep sea sediments are limited. Most works are concentrated on the northern flanks of the SCS to acquire a record of the spreading history of the SCS [40–42].

International Ocean Discovery Program (IODP) Expedition 349 aimed to establish the ages of cessation of different spreading centers in the SCS Basin [43,44]. Site U1431D was the most successful in providing a continuous archive from the Miocene to Holocene, recovering around 400 m of sediment. Since Ocean Drilling Program (ODP) Leg 184 [42], IODP 349 is one of the very few research expeditions to obtain records since the start of ocean floor spreading of the SCS basin. The acquired cores, therefore, represent a valuable archive in which age constraints for different spreading events in the sub-basins can be studied. Furthermore, the thick sediment recovery provides a continuous sedimentary record of paleoceanographic changes in the SCS. Shipboard data have been able to estimate age dates of different sections of the whole core through biostratigraphic analysis using different microfossils [43]. Calcareous nannofossils have been useful in shipboard analysis to determine sedimentation rates and estimate the cessation of the sub-basin spreading. However, further refining of datum placements is needed to achieve a better time constraint for paleoceanographic changes.

This study reinvestigates the calcareous nannofossil biostratigraphy of the Pleistocene sediments acquired from IODP 349. Temporal size and bridge angle changes in the genus *Gephyrocapsa* are discussed in detail to assess the reliability of these bioevents in the SCS. The results of the research contribute to the assessment of nannofossil datums and their importance in Pleistocene correlation and chronology, especially in the SCS.

2. Materials and Methods

2.1. Present Day Circulation of the South China Sea

Surface water circulation in the SCS is currently influenced by the EAMS [30,45,46]. The EAMS is characterized by having a stronger winter and a weaker summer season. The winter season (December–February) is dominated by the northeast monsoon, causing a basin-wide cyclonic gyre (Figure 1). The winter monsoon is mainly driven by cold winds from Siberia, which runs southward along the coast of East Asia. Mountains near the East Asian coast force the winter monsoon to produce a southwest traveling jet over the SCS. The summer season (June–August) is characterized by a weaker southwest monsoon forming an anticyclonic gyre concentrated at the south and a cyclonic cell at the

north (Figure 1). The ocean jet separates near Vietnam: one branch travels northeast crossing the central basin while the other continues on the northern path. Both branches of the current exit the SCS through the Bashi Strait. The ocean dynamics of the SCS produce localized annual upwelling in Vietnam and in northwest Luzon, although upwelling during winter is generally stronger based on chlorophyll concentrations [30,45,46].

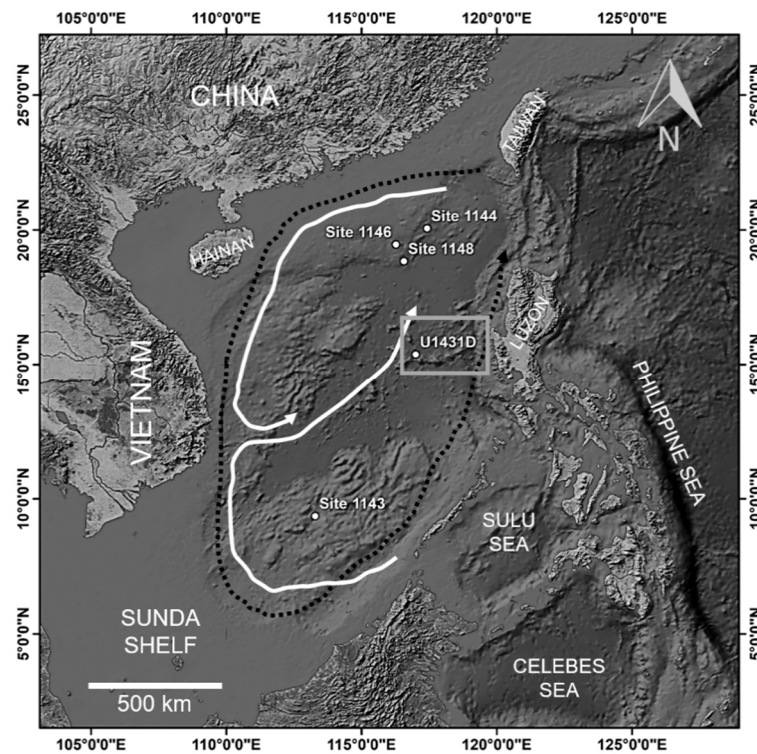


Figure 1. Site U1431 ($15^{\circ}22.5371' N$, $117^{\circ}00.0022' E$) enclosed by the box is the core used in this study. Other dots correspond to drill sites from Ocean Drilling Program (ODP) Expedition 184. The black dotted line represents the winter surface circulation of the South China Sea (SCS). The white solid line indicates summer surface circulation (modified from [46]).

2.2. Site U1431D

The sediment cores were obtained from the central SCS by IODP Expedition 349 from 1 to 6 February 2014, at Site U1431 (Figure 1). Site U1431 is located near a relict spreading ridge where the youngest magnetic anomalies in the SCS are located [43]. The primary objective of the expedition was to determine the cessation of seafloor spreading at the East Sub-basin of the SCS. The site also provides an almost continuous sediment record, providing the opportunity to study a continuous, high-resolution paleoceanographic evolution of the SCS. Core U1431D was recovered from a mean seafloor depth of 4240.5 m below sea level (mbsl). About 402.11 m of core was recovered in Site U1431D in a 617-m interval (65.2% core recovery). The uppermost 135 m of core material (from section 1H to 15H) was sampled every 20 cm for the first two sections (1H and 2H), and every 150 cm for the rest of the sections. A total of 168 samples were analyzed for this study (Figure 2).

Eleven (11) lithostratigraphic units were defined by the shipboard team based on visual core descriptions, thin section analysis, biogenic materials, and physical properties. The first two units were investigated in this study, which spans the late Pliocene (section 15H) to the latest Pleistocene (section 1H; Figure 2). Unit I (0–101.16 m below sea floor (mbsf)) is characterized by a sequence of clay, silty clay, and clayey silt that has substantially more silt than Unit II. The silt layers are composed of quartz, feldspars (plagioclases and K-feldspars), and minor amounts of amphiboles, micas, and heavy minerals. The layers with more silt are greenish gray interbeds, usually with graded, fining upward

sequences interpreted as turbidites [43]. Nannofossil oozes occur locally and often show a fining upward character, also identified as turbidite deposits. Unit I contains multiple dark gray to brown volcanic ash layers, 0.5- to 5.0-cm thick.

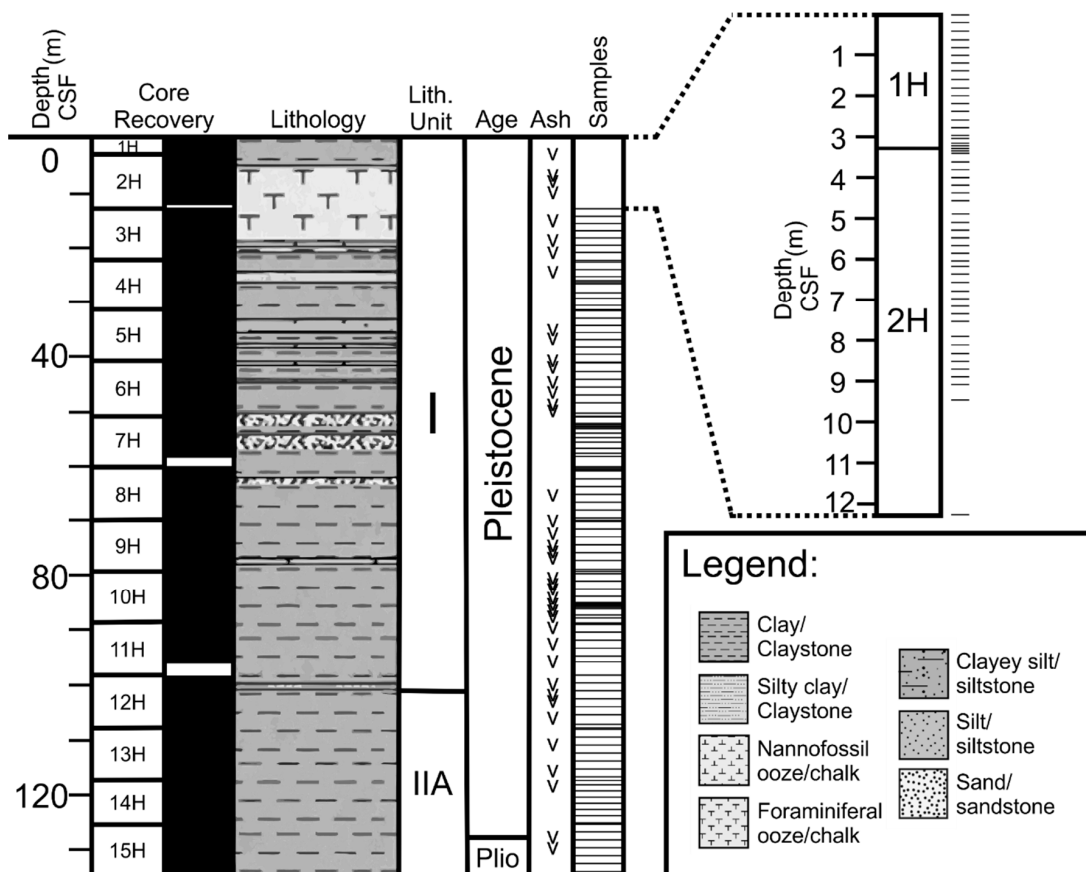


Figure 2. Schematic diagram of core sections (1H to 15H) examined in this study. It is generally composed of clays/claystone with interbeds of minor sand/sandstone, silt/siltstone, clayey silt, silty clay, and foraminiferal oozes. Age dates are determined from shipboard biostratigraphic data. White areas in the “Core Recovery” column approximates coring gaps. Horizontal lines in the “Samples” column approximate positions of the samples utilized for this study. Abbreviations listed: CSF = core depth below seafloor, H = advanced piston corer, Plio = Pliocene. Figure modified from [43].

Unit II (101.16–267.82 mbsf) is divided into two sub-units. Only samples from Sub-unit IIA (101.16–194.95 mbsf) are analyzed for calcareous nannofossils. This sub-unit is composed of clay, nannofossil-rich clay, and silty clay. The greenish gray clays are thickly bedded and are usually interbedded with greenish gray medium- to thickly-bedded nannofossil-rich clays and dark greenish gray thin- to medium-bedded silty clay layers. The clayey silt layers often show sharp, planar bases, which grade into clay and are interpreted as turbidite deposits [43]. Moreover, fine sand foraminiferal oozes with sharp, erosive bases, fining upward towards nannofossil-rich layers, are also interpreted as turbidites. Bioturbation from the *Nereites* ichnofacies are darker colored clay within lighter colored carbonate-rich sediments. Thin volcanic ash layers 0.5- to 2.0-cm thick are also identified but are much less compared to Unit I and are restricted at the upper portions of the sub-unit [43].

2.3. Calcareous Nannofossil Analysis

Smear slide replicates from unprocessed sediments were prepared following the standard procedure of [47]. At least 300 random fields of view (FOVs) were scanned using an Olympus BX51

phase contrast polarizing microscope under 1000× magnification. Additional fields of view were analyzed for samples with important calcareous nannofossil taxa. A sample was considered barren of calcareous nannofossils if there were none present after 300 FOVs. Relative abundances of individual calcareous nannofossils identified per slide were estimated using IODP standards [43]:

- D = dominant (>50%, or 100 specimens per FOV)
- A = abundant (10–50%, or 10–100 specimens per FOV)
- C = common (1–10%, or 1–10 specimens per FOV)
- F = few (0.1–1%, or 1 specimen per 1–10 FOV)
- R = rare (<0.1%, or <1 specimen per 10 FOV)

Holotypes in [48–50], supplemented by nannofossil illustrations in [6], were used for identification. Taxonomic concepts are listed in Appendix A. The calcareous nannofossil distribution is shown in the Supplementary Materials.

Nannoliths from *Discoaster* species are usually reworked specimens in younger sediments and occur both as fragmented and complete fossils within their age ranges. Thus, the last occurrences (LO) of discoasters are difficult to recognize because of reworking. Complete, incomplete, and arm fragments of 100 *Discoaster* specimens were counted from 135 mbsf to 91 mbsf to semi-quantitatively determine their relative abundances. In this study, specimens that have ≤60% of their original form intact are considered incomplete specimens. One or two arms of discoasters without a central area are considered arm fragments. The LO of the *Discoaster* is assigned to the midpoint depth between the sample containing >1% of the total count that are complete specimens and the level where it has disappeared. The informal grouping “*Discoaster* spp.” is used for ambiguous stellate nannofossils. The Base Acme (Ba) of *D. triradiatus* was identified using the definition of [51]. Based on the counts, barren intervals were noted at 133.2–130.2 mbsf, 127.5 mbsf, 124.9 mbsf, 121.9–118.9 mbsf, and 99.9–98.39 mbsf.

Morphological analysis of gephyrocapsids was done using smear slides prepared from unprocessed sediments. The *Gephyrocapsa* coccoliths were photographed and measured using Image-Pro Plus Version 7.0 mounted on an Olympus BX51 polarizing microscope under 1000× magnification. The *Gephyrocapsa* coccoliths were measured based on the parameters set by [52] (Figure 3), mainly the coccolith length and width, coccolith central area length and width, and bridge angle. At least 40 specimens per sample were analyzed. In samples with few nannofossils, 200 FOVs were scanned and all *Gephyrocapsa* placoliths seen were measured. The study adopted the biometric subdivision of [21] which is mainly based on the maximum length of the coccolith. Forms <4 μm are small *Gephyrocapsa* spp.; medium *Gephyrocapsa* spp. are those with placolith lengths from ≥4 to <5.5 μm, and large *Gephyrocapsa* spp. are ≥5.5 μm in length. All measurements are provided in the Supplementary Materials.

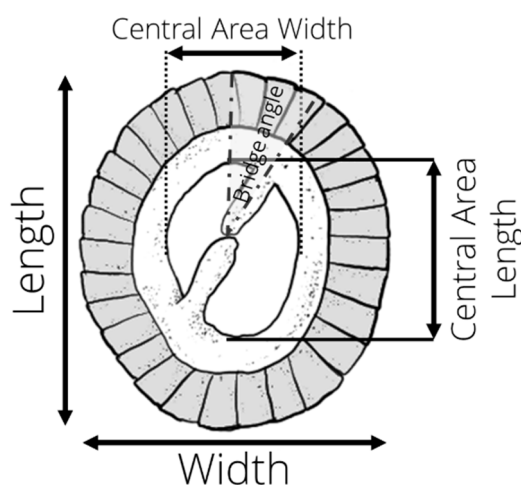


Figure 3. Measurements done on digitized photos of *Gephyrocapsa* placoliths under phase contrast research microscope at 1000× magnification.

3. Results

Twelve (12) calcareous nannofossil datums were detected for the Pleistocene section of Site U1431D. The preservation of calcareous nannofossils ranged from very poor to pristine specimens. Overgrowth and fragmentation of calcareous nannofossils (especially among discoasters) are evident. Foraminiferal tests, sponge spicules, radiolarian tests, and diatom frustules were observed in the first 3 m of the core. Samples barren of nannofossils were dominated by detrital materials such as clay minerals, biotite, plagioclase, quartz, and muscovite. Some barren intervals coincide with volcanic ash layers [43].

Calcareous nannofossil abundances were generally low throughout the core, but were high in portions of sections 1H and 2H (0 to 12.2 mbsf). Recrystallization of nannofossil specimens was uncommon throughout the core. Samples with partially to heavily dissolved placoliths coincide with decreases in calcareous nannofossil relative abundances. Figure 4 illustrates important calcareous nannofossil species used as biostratigraphic markers for Site U1431D. Table 1 summarizes all calcareous nannofossil biostratigraphic events documented in Site U1431D. The calcareous nannofossil distribution for all samples analyzed in Site U1431D is provided in the Supplementary Materials.

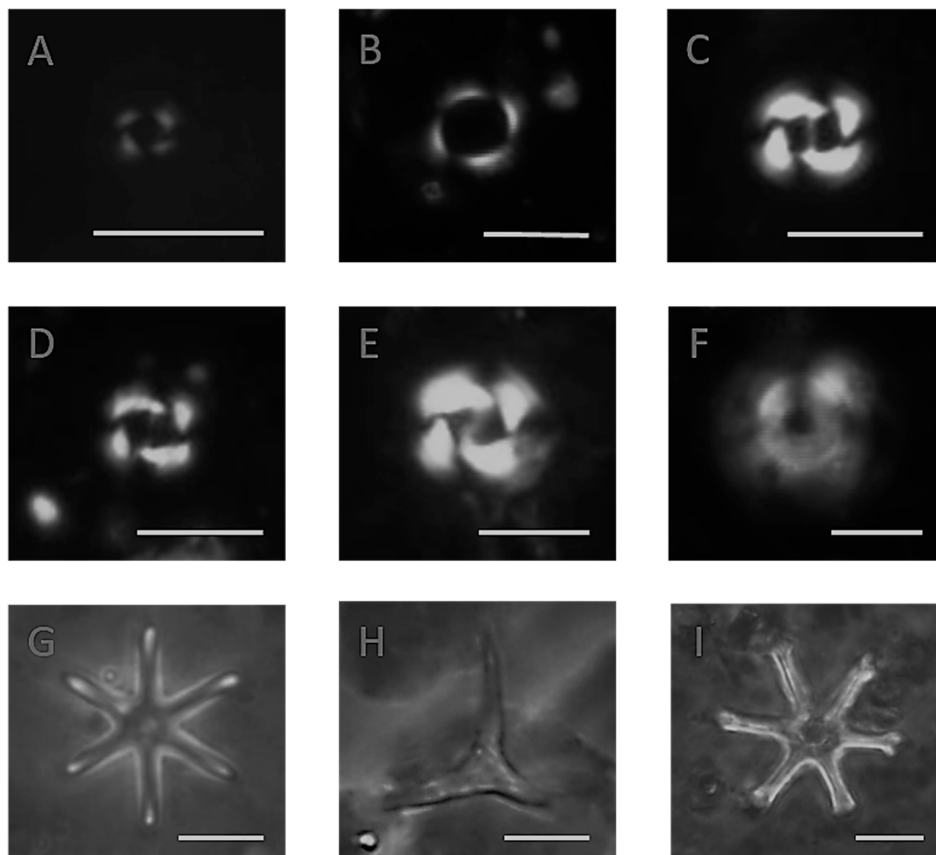


Figure 4. Photomicrographs of calcareous nannofossil marker taxa used in subdividing the uppermost Pliocene and Pleistocene. All specimens are photographed under 1000× magnification. Abbreviations listed: XPL = cross-polarized light image. PC = phase contrast image. (A) *Emiliania huxleyi*, XPL. Sample 2H-1W, 60–61 cm. (B) *Pseudoemiliania lacunosa*, XPL. Sample 2H-2W, 80–82 cm. (C) *Gephyrocapsa* sp. 3, XPL. Sample 4H-4W, 20–21 cm. (D) *Gephyrocapsa* spp. >4 μm, XPL. Sample 7H-4A, 20–21 cm. (E) *Gephyrocapsa* spp. >5.5 μm, XPL. Sample 8H-1W, 50 cm. (F) *Calcidiscus macintyreii*, XPL. Sample 10H-6W, 20–21 cm. (G) *Discoaster brouweri*, PC. Sample 12H-6W, 20–21 cm. (H) *Discoaster triradiatus*, PC. Sample 13H-7W, 20–21 cm. (I) *Discoaster surculus*, PC. Sample 15H-3W, 20–21 cm. White scale bar at the lower right of each photomicrograph is 5 μm in length.

Table 1. Summary of calcareous nannofossil biostratigraphic events of [43] and this study for International Ocean Discovery Program (IODP) Expedition 349, Site U1431D. Age discrepancies from [43] are due to the incorporation of Equatorial Pacific ages (compiled by [9]) when available. Abbreviations listed: FO—first occurrence, LO—last occurrence, Ba—base acme, reemG—reentrance event of medium *Gephyrocapsa*, tlG—top (last occurrence) of large *Gephyrocapsa*, blG—base (first occurrence) of large *Gephyrocapsa*, bmG—base of medium *Gephyrocapsa*.

IODP Expedition 349 Shipboard Results [43]			This Study		
Age (Ma)	Depth (mbsf)	Nannofossil Event	Age (Ma)	Depth (mbsf)	Nannofossil Event
0.29	3.15	FO <i>Emiliana huxleyi</i>	0.29	3.905	FO <i>Emiliana huxleyi</i>
0.44	12.15	LO <i>Pseudoemiliana lacunosa</i>	0.44	5.42	LO <i>Pseudoemiliana lacunosa</i>
0.61	32.08	LO <i>Gephyrocapsa</i> sp. 3	0.61	25.925	LO <i>Gephyrocapsa</i> sp. 3
1.02	39.67	FO <i>Gephyrocapsa</i> sp. 3	1.026	57.605	FO <i>Gephyrocapsa</i> sp. 3
1.04	50.90	reemG	1.034	58.24	reemG
1.24	60.70	tlG	1.062	60.60	tlG
1.60	89.01	LO <i>Calcidiscus macintyreii</i>	1.541	78.985	blG
1.62	96.10	blG	1.738	85.705	LO <i>Calcidiscus macintyreii</i>
			1.789	87.635	bmG
1.93	107.57	LO <i>Discoaster brouweri</i>	1.905	94.15	LO <i>Discoaster brouweri</i>
2.22	116.85	Ba <i>Discoaster triradiatus</i>	2.337	115.905	Ba <i>Discoaster triradiatus</i>
2.49	135.20	LO <i>Discoaster surculus</i>	2.491	127.855	LO <i>Discoaster surculus</i>

3.1. Calcareous Nannofossil Biostratigraphy

3.1.1. LO of *Discoaster surculus*

The LO of *D. surculus* was previously assigned to Sample 15H-CC (135.20 mbsf) in the IODP 349 biostratigraphic results [43]. Rare to few specimens are observed from Sample 15H-CC to Sample 15H-3W until they occur sporadically as reworked specimens throughout the younger portions of the sediment record (Figure 5A). There is a barren interval of nannofossils from 133.2 to 130.2 mbsf, but *D. surculus* reappeared as well-preserved specimens above this interval (Sample 15H-3W). It again reappears at 112.4 mbsf, but is regarded as reworked in this sample because not only is it higher than that of the bottom acme of *D. triradiatus*, a younger datum (Figure 5A), but its occurrence is also anomalously located above samples with consistent absences of *D. surculus*. Thus, the LO of *D. surculus* is placed between Samples 15H-3W, 20 to 21 cm and 15H-2W, 20 to 21 cm (127.85 mbsf).

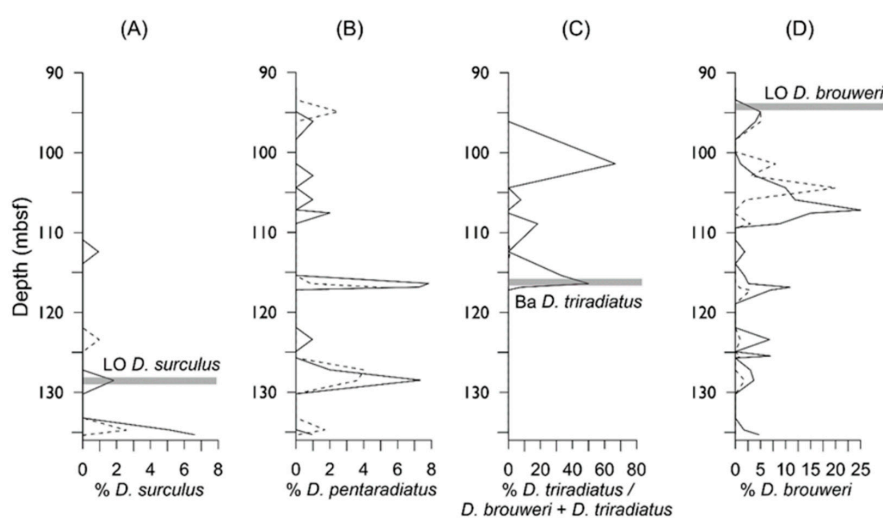


Figure 5. Relative percentages of (A) *Discoaster surculus*, (B) *D. pentaradiatus*, (C) *D. triradiatus*/*D. brouweri* + *D. triradiatus*, and (D) *D. brouweri* with depth. Highlighted portions approximate the position of the datum from biostratigraphic data. Solid lines denote complete specimens while broken lines signify incomplete specimens. Abbreviations listed: LO—last occurrence, Ba—base acme.

3.1.2. LO of *Discoaster pentaradiatus*

The occurrence of *D. pentaradiatus* is very sporadic as they occur as complete and fragmented specimens throughout the deeper sections of the core (Sample 11H-CC to Sample 15H-CC; from 96 to 135 mbsf; Figure 5B). The LO of *D. pentaradiatus* may lie between 120 and 125 mbsf based on the sharp decrease in abundance between these depth intervals and the relative placement of the LO of *D. surculus* and Ba *D. triradiatus*. However, there is a pervasive occurrence of fragmented specimens above and below this depth. Similar problems regarding the LO of *D. pentaradiatus* is also reported in ODP 149 in the Iberia Margin (Holes 897C and 898A, [53]) and Deep Sea Drilling Project (DSDP) Site 662 of the eastern North Atlantic [10]. Based on discoaster counts for Site U1431D, the LO of this species is unclear and therefore not utilized in this study.

3.1.3. Base Acme (BA) of *Discoaster triradiatus*

Relative percentages based on counts of *D. triradiatus* against *D. brouweri* have been used in determining the base acme (>20%) of the former [51]. Counts at Sample 13H-7W (116.41 mbsf) show the first increased abundance of well-preserved specimens (Figure 5C). Because *D. triradiatus* was not observed below Sample 13H-CC (116.9 mbsf), the sudden increase of well-preserved specimens in Sample 13H-7W is considered the base acme event. Above 110 mbsf (Sample 13H-1W), *D. triradiatus* also increases in abundance greater than that of Sample 13H-7W. However, the paucity of well-preserved species and the abundance decrease of *D. triradiatus* from Sample 13H-6W to Sample 13H-2W (115–110 mbsf) make extending the acme event to younger sediments questionable (Figure 5C). Thus, this datum is placed at 115.905 mbsf, between Sample 13H-7W, 20–21 cm (116.41 mbsf) and Sample 13H-6W, 20–21 cm (114.91 mbsf).

3.1.4. LO of *Discoaster brouweri*

A steady decrease in complete *Discoaster brouweri* and increase in fragmented specimens are noted from the initial placement of the datum (Sample 12H-CC; 107.57 mbsf) until its complete absence in Sample 12H-2W, 20–21 cm (99.9 mbsf; Figure 5D). Only one complete specimen is found in 12H-3W, 20–21 cm (101.4 mbsf), probably due to decreased nannofossil abundance. Samples 12H-2W, 20–21 cm (99.9 mbsf) and 12H-1W, 19–20 cm (98.39 mbsf) are nearly barren of calcareous nannofossils. However, two consecutive samples above Sample 12H-1W (Sample 11H-5-CC, 140–145 cm; 96.10 mbsf and 11H-5W, 20–21 cm; 94.9 mbsf) still contain at least 2–3% *D. brouweri*. The species is absent in Sample 11H-4W, 20–21 cm (93.4 mbsf), and in four consecutive younger samples (6 m above Sample 11H-4W). Therefore, the LO of *D. brouweri* is reassigned between Sample 11H-5W, 20–21 cm (94.9 mbsf) and Sample 11H-4W, 20–21 cm (94.15 mbsf) from Sample 12H-CC (107.57 mbsf; [43]; Figure 5D).

3.1.5. First Occurrence (FO) of Medium *Gephyrocapsa* spp. (bmG)

The base of medium *Gephyrocapsa* (bmG) lies between Samples 10H-7W, 22 to 23 cm and 10H-8W, 20 to 21 cm (87.635 mbsf), which was previously unreported in shipboard results [43]. Placolith length measurements have been useful in determining the nannofossil datum. The *gephyrocapsid* specimens observed generally have a bridge oriented nearer the long axis of the coccolith (15°–40°) and a relatively open central area. These *gephyrocapsids* are most likely equivalent to *Gephyrocapsa oceanica*, *G. margereli*, and *G. muelleriae*.

3.1.6. LO of *Calcidiscus macintyreii*

The species *C. macintyreii* generally occurs sporadically (only 1 or 2 specimens) in Sample U1431D-15H-CC, 10–16 cm to 7H-6W, 20 to 21 cm (135.33 to 57.9 mbsf), except in Samples 14H-CC (125.48 mbsf) and 10H-6W, 20 to 21 cm (85.8 mbsf) where they occur as few specimens. Recognition of *C. macintyreii* above Sample 10H-CC is difficult because siliciclastic materials dominate the samples and nannofossils are reworked to younger portions of the core. Coccolith preservation is moderate to good

in Samples 10H-CC to 10H-6W, while very few, poorly preserved and broken specimens of *C. macintyreii* are found above the interval and occur sporadically in younger sediment samples. Furthermore, coccoliths ~9 µm but similar to the morphology of *C. macintyreii* are noted in some samples. In this study, the last occurrence is placed between Samples 10H-6W, 20 to 21 cm and 10H-5W, 20 to 21 cm (85.705 mbsf).

3.1.7. FO of Large *Gephyrocapsa* spp. (blG)

The base (first occurrence) of large *Gephyrocapsa* (blG) had been documented at Sample U1431D 11H-CC (98.15 mbsf) based on IODP shipboard biostratigraphy (Li et al., 2014). However, this study did not observe large *Gephyrocapsa* at any sample within sections 11H and 10H (from 96.10 to 79.40 mbsf). It is detected much shallower (at Samples 9H-CC (78.91 mbsf) and above) and occurs above the LO of *C. macintyreii* rather than below it. Few to common large *Gephyrocapsa* specimens occur at Sample 9H-CC (78.91 mbsf) and they appeared abruptly in the sediment record. The first occurrence of large *Gephyrocapsa* morphotypes has also been documented above the LO of *C. macintyreii* in the Shatsky Rise in the northwest Pacific Ocean [54] and in ODP Leg 111 [55] and ODP Leg 138 [56] in the Equatorial Pacific. This pattern is also seen in the Caribbean Sea from ODP Leg 165 [57] and in the South Atlantic at ODP Sites 925 and 926 [58]. Thus, the blG is placed between Samples 9H-CC and 9H-7W, 36 cm (78.985 mbsf), above the LO of *C. macintyreii*. The distinct first appearance of large *Gephyrocapsa* suggests that they are reliable markers in the SCS.

3.1.8. LO of Large *Gephyrocapsa* spp. (tlG)

The LO of large *Gephyrocapsa* (>5.5 µm) was reported in Sample U1431D 8H-1W, 50 cm (60.70 mbsf; [43]). Very good coccolith preservation is observed in this sample. Samples above and below this interval (8H-1W, 40 to 41 cm, 8H-1W, 20 to 21 cm and 8H-2W, 19 to 20 cm, respectively) are barren of nanofossils while Sample 7H-CC has no large *Gephyrocapsa*. Thus, the LO lies between Samples 8H-1W, 50 cm and 8H-1W, 40 to 41 cm (60.65 mbsf), and is consistent with shipboard results [43].

3.1.9. Reentrance Event of Medium *Gephyrocapsa* spp. (reemG)

Measurements of *Gephyrocapsa* coccoliths recognized the reentrance event of medium *Gephyrocapsa* (reemG) in Sample 7H-6W, 20 to 21 cm (57.90 mbsf). The placoliths are characterized by generally high bridge angle values (60°–70°) but are not exactly parallel to the short axis. The reemG is reassigned between Samples 7H-CC, 24 to 29 cm and 7H-6W, 20 to 21 cm (58.24 mbsf) from Sample 6H-CC reported in shipboard results (50.90 mbsf; [43]). In Site U1431D, the reemG event does not exactly correspond to the first occurrence (FO) of the omega-type *Gephyrocapsa* (*Gephyrocapsa* sp. 3). This trend is also observed in ODP 198, Site 1209B, in the Shatsky Rise [59] and in ODP 161 in the western Mediterranean [60].

3.1.10. FO and LO of *Gephyrocapsa* sp. 3

The FO of *Gephyrocapsa* sp. 3 was initially observed at Sample U1431D 5H-6W, 47 cm (39.67 mbsf; [43]). The occurrence of *Gephyrocapsa* sp. 3 in the sediment core shows a cyclical appearance and disappearance of nanofossils. Detrital material seen in smear slides probably diluted the nanofossil content. These barren layers are punctuated by samples with well-preserved, abundant calcareous nanofossils. The refinement of nanofossil biostratigraphy extended the FO further downcore to Sample 7H-5W, 60 to 61 cm (57.30 mbsf). The FO of *Gephyrocapsa* sp. 3 is then placed between Samples 7H-5W, 60 to 61 cm and 7H-6W, 20 to 21 cm (57.60 mbsf). This datum is 60 cm above the reemG event in Site U1431D. The LO of this nanofossil was initially placed at Sample U1431D 4H-CC, 29 to 34 cm (32.08 mbsf; [43]). The results of this study show that the LO is found between Samples 4H-3W, 20–21 cm, and 4H-3W, 120 to 121 cm (25.925 mbsf).

3.1.11. LO of *Pseudoemiliania lacunosa*

Shipboard results from IODP Site U1431D placed the LO of *P. lacunosa* at Sample 2H-CC, 0 to 4 cm (12.15 mbsf; [43]). In this study, the datum is found at younger portions of the core—between Samples 2H-2W, 80 to 82 cm and 2H-2W, 60 to 62 cm (5.42 mbsf). Circular morphotypes are found more abundantly in the deeper sections of the core, while elliptical types are more common in younger sediments. Only the elliptical forms of *Pseudoemiliania* are documented in the last two samples (Samples 2H-2W, 100 to 102 cm and 2H-2W, 80 to 82 cm; 5.7 and 5.5 mbsf, respectively).

3.1.12. FO of *Emiliania huxleyi*

The FO of *E. huxleyi* was previously reported at Sample 1H-CC, 7 to 14 cm (3.22 mbsf; [43]). The datum has been reassigned between Samples 2H-1W, 60 to 61 cm and 2H-1W, 80 to 81 cm (3.905 mbsf). Nannofossils above and below the event show a cyclical trend of barren and well-preserved assemblages, which made the recognition of this bioevent difficult. Dissolution in some of the nannofossils, especially among the placoliths, is also observed.

3.2. Morphologic Changes in *Gephyrocapsa* in Site U1431D

Small *Gephyrocapsa* is the only morphotype present from 135 to 87.94 mbsf (~2.58 to 1.79 Ma). It is characterized by a large central area and has varying bridge angles, although low average values are recorded in the interval. The overall trend shows an increasing small *Gephyrocapsa* coccolith length throughout the core. Medium *Gephyrocapsa* first appeared at 87.635 mbsf (~1.79 Ma) and does not show any long-term changes in length. The increase in the length of medium forms corresponds to an increase in the overall length of small morphotypes throughout most of the interval (Figure 6). Large *Gephyrocapsa* occurs consistently only from 78.91 to 60.70 mbsf. Exceptionally large forms (between 7.5 and 8.0 μm) are documented at around 0.8 Ma. No observable long-term trends in size changes are noted for the large morphotypes.

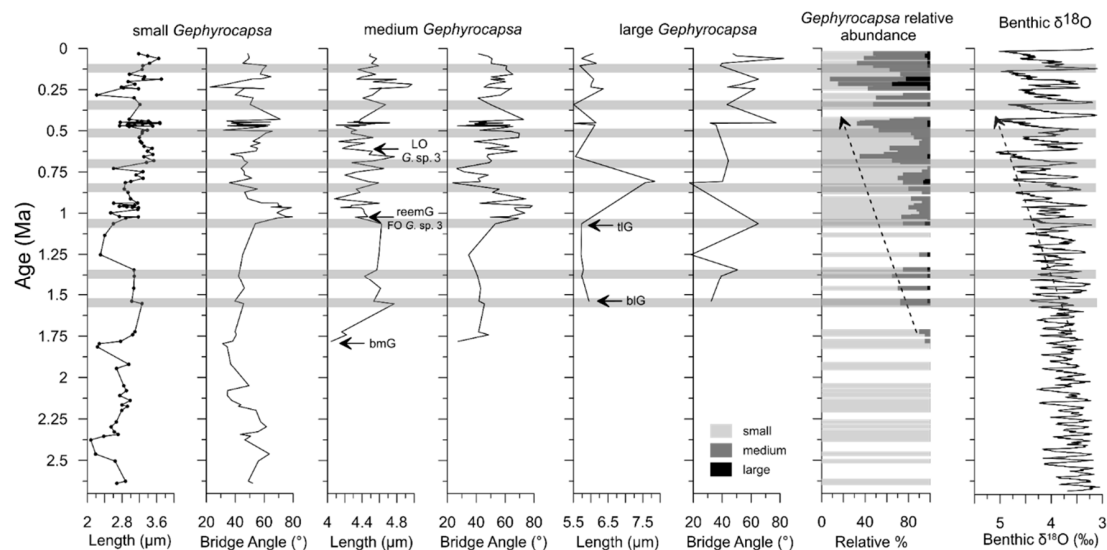


Figure 6. Size measurements of *Gephyrocapsa* from Site U1431D correlated with the LR04 Stack of [2]. Dots in the leftmost line graph are sample points. Gray bars highlight onsets of relative abundance peaks in medium *Gephyrocapsa* forms. Blank intervals in the relative abundance graph indicate barren samples. The age of each sample was calculated through linear interpolation of data points following the results of nannofossil biostratigraphy. The dashed arrows in the relative abundance graph and LR04 Stack show trends in increasing amplitude fluctuations. Abbreviations listed: LO—last occurrence, FO—first occurrence, reemG—reentrance event of medium-sized *Gephyrocapsa*, tIG—top of large *Gephyrocapsa*, blG—base of large *Gephyrocapsa*, bmG—base of medium *Gephyrocapsa*.

Bridge angle changes across the *Gephyrocapsa* morphotypes range from 30° to 75° (Figure 6). A general decrease in bridge angle is documented from 2.58 to 1.79 Ma (small *Gephyrocapsa*) while an increase in bridge angle from 1.79 to 0.9 Ma is evident in the record (small and medium *Gephyrocapsa*). The highest values for bridge angles for small and medium forms are noted from 1.04 to 0.9 Ma and correlate with the first occurrence of *Gephyrocapsa* sp. 3. The bridge angle rapidly decreases in value from 0.9 to 0.8 Ma. An overall increase in bridge angle is seen from 0.8 Ma to present, with distinct lows between 0.5 and 0.45 Ma and at 0.2 Ma. In general, the bridge angle changes seem to respond similarly, regardless of the size fraction, and there is no apparent relation between the bridge angle with respect to average placolith length (Figure 6).

Relative abundances of small, medium, and large *Gephyrocapsa* morphotypes show oscillations in relative abundances of small and medium forms at around 1.79 and 0.65–0.6 Ma (Figure 6). Medium *Gephyrocapsa* comprise 20–30% of the total *gephyrocapsid* assemblage in this interval. From 0.65 to 0.6 Ma, oscillations of the shifting dominance of small and medium forms became more evident. When medium *Gephyrocapsa* is dominant, large morphotypes also appear in the record in few numbers, except for a spike in large *Gephyrocapsa* at around 0.2 Ma. The increasing amplitude fluctuation of medium *Gephyrocapsa* roughly coincides with the increasing glacial–interglacial variations trending towards younger sections (Figure 6). However, it is not clear if the driving mechanism of the changes in relative abundance fluctuations is correlated to glacial or interglacial stages, as both increasing and decreasing trends are evident in both conditions.

4. Discussion

4.1. Magnetobiochronologic Calibration of Nannofossil Datums in Site U1431D

Nannofossil events identified in Site U1431D are tied with magnetostratigraphic data from shipboard results to estimate a numerical age for the calcareous nannofossil datums. Magnetostratigraphic reversals are calibrated against [61], compiled in [9], while the calculation of the numerical ages using magnetostratigraphy is explained in the Supplementary Materials. Low- to mid-latitude Deep Sea Drilling Project (DSDP) and ODP sites are utilized to compare the nannofossil ages of datums observed in Site U1431D. The locations of these DSDP and ODP Sites are listed in Table 2 and are shown in Figure 7. The magnetobiochronologic calibrations are mostly in agreement with the compilation of [9], except for some datums (Table 1). These inconsistencies are focused on the discussion below.

Table 2. Location of Deep Sea Drilling Project (DSDP), ODP Sites, and onshore references used for comparison.

Hole/Name	Latitude	Longitude	Water Depth (m)	Reference(s)
DSDP 552	56°02.56' N	23°13.88' W	2301	[13,62]
DSDP 607	41°00.07' N	32°57.44' W	3427	[21,22,63]
ODP 964	36°15.62' N	17°45.025' E	3650	[64]
Boso Peninsula	35° N	140° E	-	[65]
ODP 1146	19°27.40' N	116°16.37' E	2092	[42]
ODP 1148	18°50.17' N	116°33.93' E	3294	[42,66]
ODP 769B	8°47.12' N	121°17.68' E	3644	[67]
ODP 768B	8°00.05' N	121°13.19' E	4385	[67]
ODP 925B	4°12.25' N	43°29.35' W	3041	[58]
ODP 677	1°12.03' N	83°44.16' W	3461	[21,22]
ODP 848	2°59.6' S	110°28.8' W	3855	[68]
ODP 710	4°18.7' S	60°58.8' E	3824	[13,69]
DSDP 593	40°30.47' S	167°40.47' E	1068	[70,71]

The LO of *Calcidiscus macintyreii* in Pacific, Atlantic, Indian, and Mediterranean sections are correlated to Chron C1r.3r; however, the placement of the datum within the chron varies by location

(Figure 8). Excluding Site 1146, the Indian, Atlantic, and Mediterranean records have younger age estimates than the Pacific and the SCS. In Site U1431D, correlation with shipboard magnetostratigraphy suggests that the event falls just above the top of the Olduvai Chron (C2n; 1.778–1.945 Ma, [9]), but still within the lowermost portions of Chron C1r.3r, while previous works document the LO of *C. macintyreii* at a slightly higher magnetostratigraphic position (lower C1r.3r but not directly on top of Olduvai—[7,9,22,58,64,70–72]). Discrepancies in the ages of the extinction event (0.2 Ma) may suggest diachroneity.

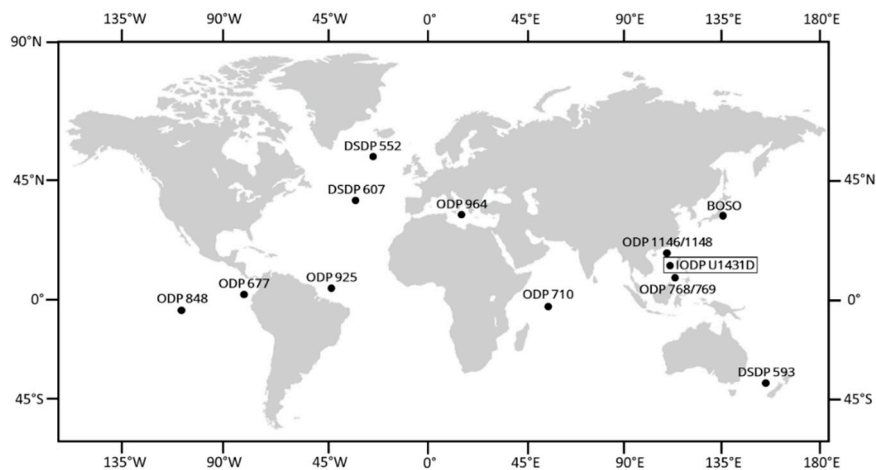


Figure 7. Location of DSDP/ODP/IODP Sites used in this study for comparison of Pleistocene nannofossil datums. Site IODP 1431 is examined in the present study.

Although the taxonomic definition of *C. macintyreii* is simple, several inconsistencies and differing species concepts exist in the literature. In Sites 768 and 769 in the Sulu Sea, [67] cited [73] for their adopted age for *C. tropicus* to subdivide NN19 of [74]. However, there is no written account of *C. tropicus* in [73]. The *C. tropicus* of [67] may be equivalent to the *C. macintyreii* of [73]. This equivalence may be unlikely because large age discrepancies exist in the literature between the two species (1.48 Ma—[67]; 1.57 Ma—[73]) and thus the differences may be an effect of varying species concepts. The stratigraphic inconsistency for the datum is also reported in the Japan Sea (1.33 Ma; [75]). The LO in the Japan Sea is younger by 0.22 Ma compared to the study of [51] and by 0.27 Ma compared to [7]. Size variations in *C. leptoporus* (5–8 μm , sometimes reaching up to 10 μm) may have caused confusion whether the larger end of the species belonged to *C. macintyreii* or a larger variant of *C. leptoporus* (e.g., [75]).

Studies concerning the LO of *Gephyrocapsa* sp. 3 are limited only to the Mediterranean. The limited occurrence and distribution of studies of the LO of *Gephyrocapsa* sp. 3 is the reason [7] did not include the event for global biostratigraphic correlation. The datum age (0.58 Ma) was first identified by [76] and calibrated through magnetostratigraphy. More recent calibrations in the Mediterranean correlated the event to MIS 15 (0.570–0.577 Ma; [64,77]). In the SCS, there is very little documentation on the distribution of this nannofossil downcore [43]. The LO of *Gephyrocapsa* sp. 3 is placed within the middle portions of Chron C1n (Brunhes Chron; 0–0.780 Ma) in Site U1431D, suggesting an age of 0.44 Ma for the datum (Figure 9). Although events using *Gephyrocapsa* are used in some studies in the SCS [41,42], this study presents one of the very few evidence for the occurrence and distribution of *Gephyrocapsa* sp. 3 in SCS Pleistocene sediments. Its clear appearance downcore implies its significance as a calcareous nannofossil marker in the SCS. It must be noted with caution that *Gephyrocapsa* sp. 3 is still present in the open ocean today [77]; thus, careful analysis of the bridge angles of *Gephyrocapsa* downcore may be necessary to determine the LO of this species.

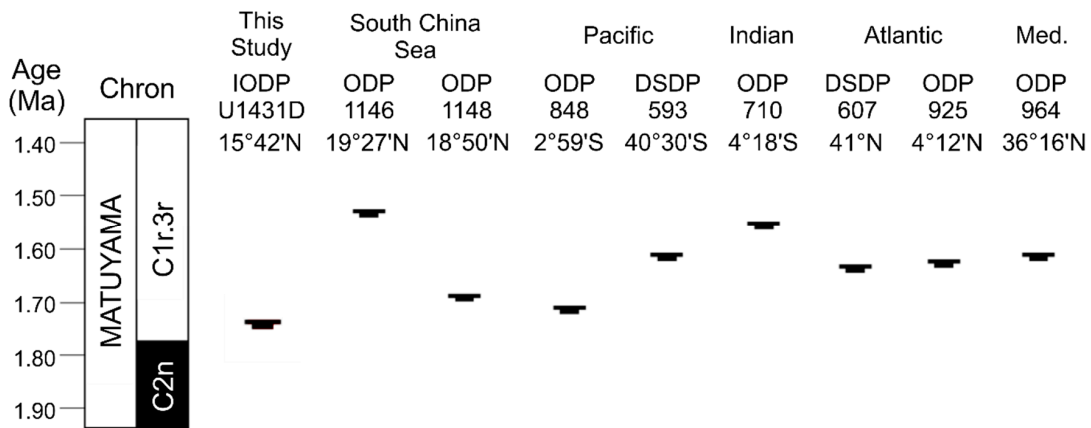


Figure 8. Comparison of stratigraphic ranges of the LO of *Calcidiscus macintyreii* from IODP/ODP/DSDP Sites. Magnetostratigraphic records from IODP Site U1431D, ODP Sites 1148, 848, 710 and DSDP Site 593 are calibrated to the astronomically tuned Geomagnetic Polarity Time Scale (GPTS) of [61] as compiled by [9]. Oxygen isotope data is used to determine the ages in ODP Sites 1146, 925, 964 and DSDP Site 607. These datums are calibrated to the benthic foraminiferal $\delta^{18}\text{O}$ time scale of [2]. Horizontal bars represent the recalculated datum ages for each site. Med.—Mediterranean. Black—normal; white—reversed polarity.

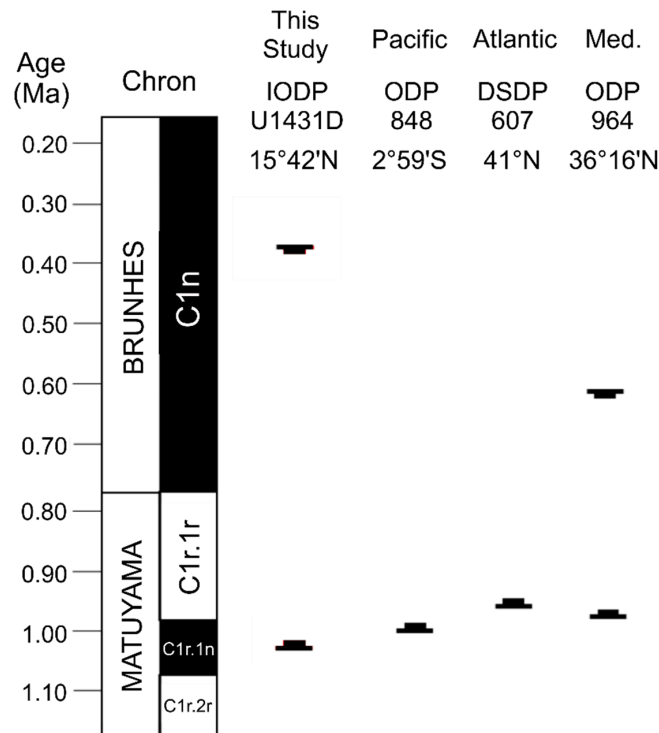


Figure 9. Comparison of stratigraphic ranges of the FO and LO of *Gephyrocapsa* sp. 3 from IODP/ODP/DSDP Sites. Magnetostratigraphic records from IODP Site U1431D and ODP Site 848 are calibrated to the astronomically tuned Geomagnetic Polarity Time Scale (GPTS) of [61] as compiled by [9]. Oxygen isotope data is used to determine the ages in ODP Site 964 and DSDP Site 607. These datums are calibrated to the benthic foraminiferal $\delta^{18}\text{O}$ time scale of [2]. Horizontal bars represent the recalculated datum ages for each site. Upward facing horizontal bars represent FO datums, while downward facing bars signify LO datums. Med.—Mediterranean. Black—normal; white—reversed polarity.

Correlation with magnetostratigraphy places the LO of *P. lacunosa* within the upper portions of Chron C1n (Figure 10), which corresponds to an age of 0.092 Ma in Site U1431D. There is a considerable age discrepancy in the LO of *P. lacunosa* in Site U1431D compared to the literature. The difference ranges from 0.37 Ma between Sites U1431D and Sites 1146 (SCS; [42]), 925 (Atlantic; [58]), and 964 (Mediterranean; [77]) to as much as 0.55 Ma compared to the southwest Pacific [74,75]. The results of this study differ significantly compared from previous works which suggest the LO of *P. lacunosa* to be correlated to MIS 12 [17,21,22]. The upper portions of the core are defined mainly by interbedded to interlaminated clayey silt to silty clay which are interpreted as turbidite sequences [43]. Turbidity currents may have caused the resuspension of coccoliths of *P. lacunosa* to younger sediments of the core. Uncertainties in magnetostratigraphic calibration may also be a factor in the age discrepancy. Because the age calculated from magnetostratigraphy is too young compared to other sites, the standard age of 0.44 Ma [9] is adopted for the LO of *P. lacunosa* (Figure 10, gray datum).

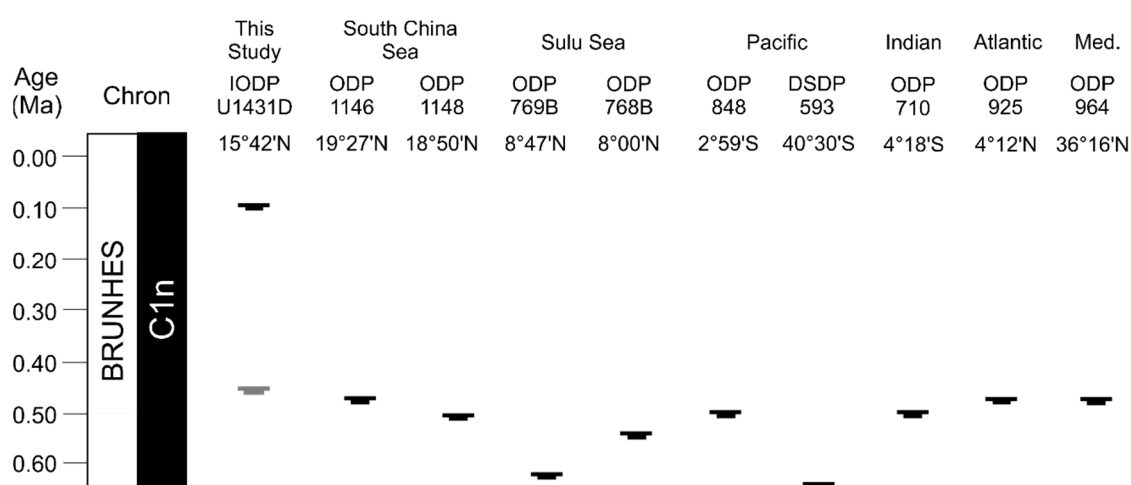


Figure 10. Comparison of stratigraphic ranges of LO of *Pseudoemiliania lacunosa* from IODP/ODP/DSDP Sites. Magnetostratigraphic records from IODP Site U1431D, ODP Sites 1148, 769B, 768B, 848, 710 and DSDP Site 593 are calibrated to the astronomically tuned Geomagnetic Polarity Time Scale (GPTS) of [61] as compiled by [9]. Oxygen isotope data is used to determine the ages in ODP Sites 1146, 925 and 964. These datums are calibrated to the benthic foraminiferal $\delta^{18}\text{O}$ time scale of [2]. Horizontal bars represent the recalculated datum ages for each site. Black datum in IODP Site U1431D represents age acquired from magnetostratigraphy. Gray datum in IODP Site U1431D represents placement of the datum from this study using the datum age reported in [9]. Med.—Mediterranean.

The age of the FO of *E. huxleyi* in Site U1431D also has a large discrepancy. Correlation to Site U1431D magnetostratigraphy showed that the FO of *E. huxleyi* corresponds to the upper portions of Chron C1n at 0.066 Ma (Figure 11, black datum). The oldest age estimates are found in ODP Sites 1146 and 1148 followed by ODP Sites 768 and 769 in the Sulu Sea (Figure 11). Younger ages are noted from the open ocean (Pacific and Atlantic) and in the Mediterranean Sea; however, the age acquired from Site U1431D is much younger than all other sites. The uncertainty ranges from 0.305 Ma compared to Site 1148 [42] to 0.188 Ma compared to Site 925 [58]. Bioturbation and terrigenous input to the basin may have affected the signal of the FO. Bioturbation causes vertical sediment mixing which may reposition a datum to a slightly deeper depth. However, shipboard results reveal only slight bioturbation (10–30%) in the interval where the FO of *E. huxleyi* is documented [43] and may have had minor effect in the position of the datum. Terrigenous input may be a problem especially for less robust species like *E. huxleyi*. Previous reports suggest the sporadic occurrence of *E. huxleyi* near its first appearance [15,17,78]. Carbonate dilution through terrigenous input might further obscure the datum. Shipboard data suggest that carbonate percentages in Pleistocene sediments of Site U1431D are very low (1–10%; [43]). This interval is also defined by an abundance of plagioclase, mica, and amphibole

seen in smear slides, suggesting increased detrital input. Magnetostratigraphic calibration may have also contributed to the age discrepancy recorded in IODP Site U1431D. Thus, the age of 0.29 Ma [9] is adopted for the datum (Figure 11, gray datum).

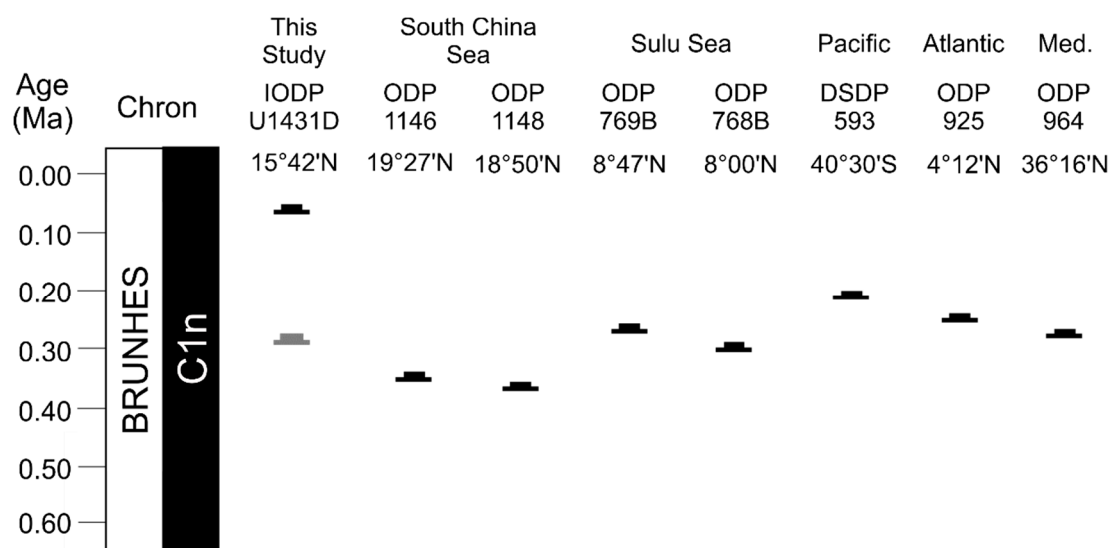


Figure 11. Comparison of stratigraphic ranges of FO of *Emiliana huxleyi* from IODP/ODP/DSDP Sites. Magnetostratigraphic records from IODP Site U1431D, ODP Sites 1148, 769B, 768B, and DSDP Site 593 are calibrated to the astronomically tuned Geomagnetic Polarity Time Scale (GPTS) of [61] as compiled by [9]. Oxygen isotope data is used to determine the ages in ODP Sites 1146, 925 and 964. These datums are calibrated to the benthic foraminiferal $\delta^{18}\text{O}$ time scale of [2]. Horizontal bars represent the recalculated datum ages for each site. Black datum in IODP Site U1431D represents age acquired from magnetostratigraphy. Gray datum in IODP Site U1431D represents placement of the datum from this study using the datum age reported in [9]. Med.—Mediterranean.

4.2. The Importance and Complexity of *Gephyrocapsa* Morphometry in Site U1431D

The overall time-transgressive size increase correlates well with those of previous works [19,21–24,59,79]. The work of [19] complements the data gathered; however, no large *Gephyrocapsa* were observed in the lower Pleistocene sections of the core studied. Only small *Gephyrocapsa* spp. placoliths are documented from Sample 15H-CC (~135.3 m; latest Pliocene) to 10H-8W, 20–21 cm (~87.94 m; early Pleistocene). The Pliocene–Pleistocene was defined at the base of the Calabrian (~1.8 Ma) by [19] and may account for the disparity. Nevertheless, the size increase is documented across ocean basins; thus, the morphologic change in *Gephyrocapsa* most probably points to an evolutionary trend. The time-transgressive size increase is applicable for biostratigraphic use and may explain the comparable record of Site U1431D sediments to other ocean basins. Global climate changes longer than glacial–interglacial cycles, such as ocean cooling brought on by a steady increase in ice cover, may have affected the long-term changes in the size of *Gephyrocapsa* coccoliths [79]. It is also noted that the changes in morphological parameters of the *Gephyrocapsa* are not in one-to-one correspondence with glacial–interglacial variations. Higher resolution sampling, correlatable to suborbital variations in $\delta^{18}\text{O}$, is needed to further explain the response of *Gephyrocapsa* during these time scales.

Specimens of *Gephyrocapsa* coccoliths analyzed by [80] from tropical Atlantic waters generally have high bridge angles (parallel to the short axis of the coccolith). This observation is supported by [52], noting further that the bridge angle may be correlated with geographic distribution—the position of the bridge approaches the long axis towards high latitudes, in contrast to a mean bridge angle of 60° within 15 degrees north and south of the Equator. If temperature has a direct effect on bridge angle orientation, then there should be a glacial–interglacial trend with respect to bridge angle, with relatively colder periods shifting to lower bridge angle values. However, in Site U1431D there is

very little correlation between the average bridge angle values of all size fractions measured and the $\delta^{18}\text{O}$ record (LR04 Stack of [2]; Figure 6). Most probably, environmental factors other than temperature may have had an influence on the development of the bridge.

The presence of medium-sized forms with high bridge angle values at around 1.0–0.6 Ma is documented in this study and is comparable to previous works [7,19,21,23,24,59,81–83]. This *Gephyrocapsa* morphotype is most probably equivalent to *Gephyrocapsa* sp. 3 of [19], *Gephyrocapsa oceanica* vertical of [23], and *Gephyrocapsa* sp. C of [24]. Small forms of *Gephyrocapsa* with a bridge angle parallel to the short axis are also documented mostly from 1.0 to 0.9 Ma near the “small *Gephyrocapsa acme*” [23,24]. These studies are correlatable and span different ocean basins, each with their own local climate. Thus, the changes in the morphology of *Gephyrocapsa* in the SCS may not be factors of regional climate perturbations. These results show the importance of both bridge angle and size for the determination of certain *Gephyrocapsa* morphotypes for Pleistocene biostratigraphy.

4.3. Age–Depth Model for Site U1431D

An age–depth model is constructed based on magnetostratigraphic and nannofossil datums identified in Site U1431D. The datum ages are calculated based on linear interpolation between magnetostratigraphic chrons (Supplementary Materials). The ages for the FO of *E. huxleyi* and LO of *P. lacunosa* are adopted from [9] because the calculated site-specific ages are too young compared to published figures. The LO of *Gephyrocapsa* sp. 3 is also taken from [9] because the only calibration done for this datum is from [76] and [64] in the Mediterranean. Thus, the age–depth model for Site U1431D is a combination of ages compiled by [9] and site-specific numerical ages.

The age–depth curve generated from the nannofossil datums using calcareous nannofossils shows consistency with other microfossil groups (Figure 12). From 135 mbsf to ~80 mbsf, planktonic foraminifera and calcareous nannofossil data generally agree with each other (Figure 12), with slight divergence at the 100–135 mbsf interval. Above 90 mbsf, planktonic foraminiferal datums imply younger ages than the calcareous nannofossils. Further analysis of planktonic foraminiferal biostratigraphy is needed to verify the age discrepancies between the two microfossil groups. The age model from radiolarians for the uppermost layers (0–10 mbsf) agrees with the nannofossils, reflecting a slow sedimentation rate within the interval.

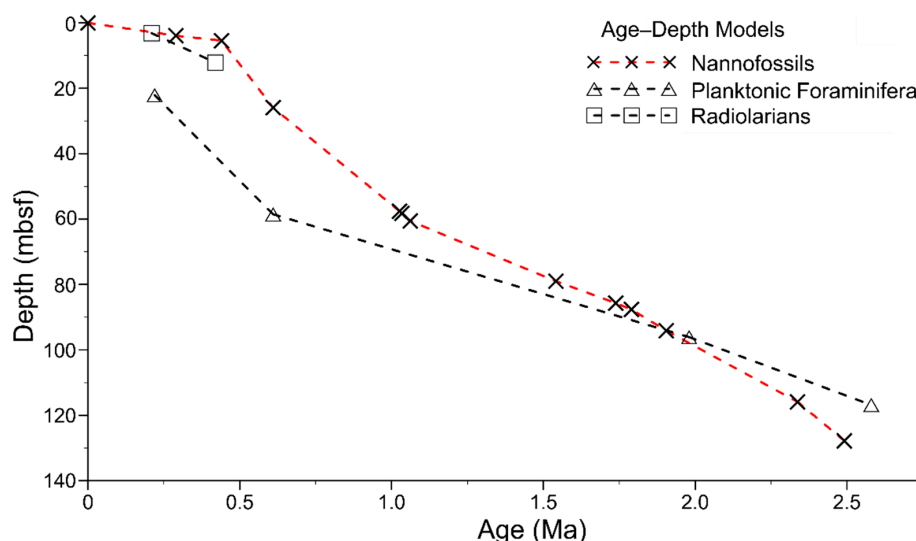


Figure 12. Comparison of age–depth models using different microfossil groups for Site U1431D. Symbols represent specific microfossil groups found in the site. The nannofossil age model incorporates published ages for FO of *E. huxleyi*, LO of *P. lacunosa*, and LO of *Gephyrocapsa* sp. 3 found in [9] and magnetostratigraphic ages acquired from this study for the older datums. The planktonic foraminifera and radiolarian curves use the ages from [9].

The sedimentation rate in Site U1431D may be divided into three distinct segments based on nannofossil datums (Figure 12). From 135 to 60.6 mbsf, the estimated sedimentation rate is ~46.7 m/Ma, representing the time frame between 2.49 to 1.06 Ma. Sedimentation rates almost doubled from 60.6 to 5.42 mbsf, estimated at about 85.2 m/Ma. This period of high sedimentation characterizes the interval between 1.06 and 0.44 Ma. A very slow sedimentation rate of ~12.7 m/Ma occurred after 0.44 Ma.

4.4. Other Possible Nannofossil Events

There are other possible nannofossil events found in the core which may need further reexamination. These events are recorded as shifts in the abundance values of nannofossil species, or a cross-over of the abundance of variants within a species. These shifts may offer biostratigraphic significance if assessed further and documented across other basins.

The genus *Pseudoemiliana* had been differentiated based on the number of distal slits [23] and the degree of ellipticity [84]; these morphotypes are not routinely used in biostratigraphy. However, large, circular forms only appeared in the late Pleistocene and the changes in their morphology may be related to temperature fluctuations [48,85]. Absolute abundance counts from Site U1431D show a shift in abundance between *Pseudoemiliana* circular and elliptical variants between 120 to 130 mbsf (Figure 13). Circular variants of *P. lacunosa* are dominant from 135 to 130 mbsf and become replaced by elliptical types. This observation is different from the work of [84] wherein the circular forms of *Pseudoemiliana* dominate the younger portions of DSDP Leg 4 cores. It is possible that ecological preferences and the marginal basin setting of the SCS may have affected the distribution of *Pseudoemiliana* compared to the open-ocean setting of DSDP Leg 4 [84].

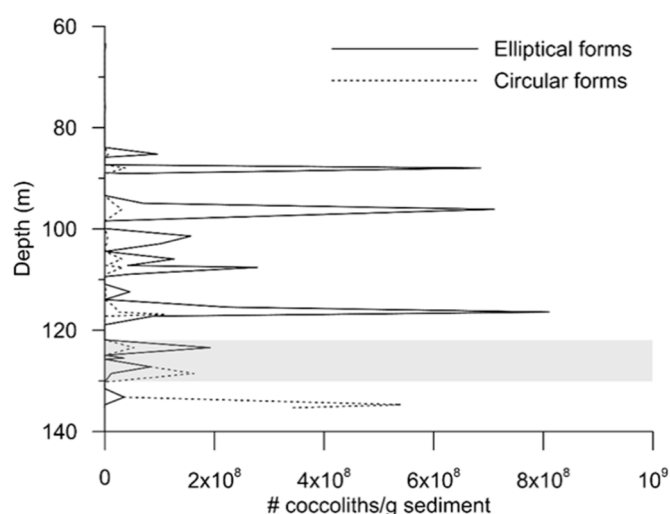


Figure 13. Absolute abundance of the calcareous nannofossil *Pseudoemiliana lacunosa* from 0 to 135 mbsf. Broken line shows abundance of circular variants. Solid line shows abundance of elliptical morphotypes. The gray highlighted area estimates the transition of circular-dominated to elliptical-dominated *Pseudoemiliana* in the core.

The first and last occurrences of the small *Gephyrocapsa* acme (1.24 to 1.02 Ma, respectively [9]), was not detected in Site U1431D. Possible carbonate dilution through terrigenous input may have been the cause of the absence of the event. However, Zone NN21 [74] consists of several other *Gephyrocapsa* acme intervals, one of which may be recorded in the SCS. Nannofossil biostratigraphy from the Kings Trough at the northeastern Atlantic Ocean show several acme intervals corresponding to different species of small *Gephyrocapsa* [85]. They have documented the dominance of *G. aperta* near the FO of *E. huxleyi*. In Sample 2H-1W, 60–61 cm (3.80 mbsf), an increase in small *Gephyrocapsa* placoliths is observed (Figure 14). These small placoliths have a large central area and a bridge near the long

axis, in agreement with the taxonomic description of *G. aperta*. Interestingly, the first occurrence of *E. huxleyi* is assigned to this sample and correlates well with observations in Kings Trough. A minor small *Gephyrocapsa* acme event occurs between Zones NN20 and NN21 [86] and was also documented by [24], most likely corresponding to the earlier portions of their Assemblage “B”.

The reliability of these secondary events can be assessed through correlation with oxygen isotope stratigraphy or cyclostratigraphy using the physical properties of sediments in the SCS. These minor events have been noted in some studies [24,84–86]. Details of these events in the SCS can be studied further through higher resolution sampling in the intervals where they are noted. Additional data from other ocean basins are needed to verify whether these nannofossil events are recorded on a regional or a global scale.

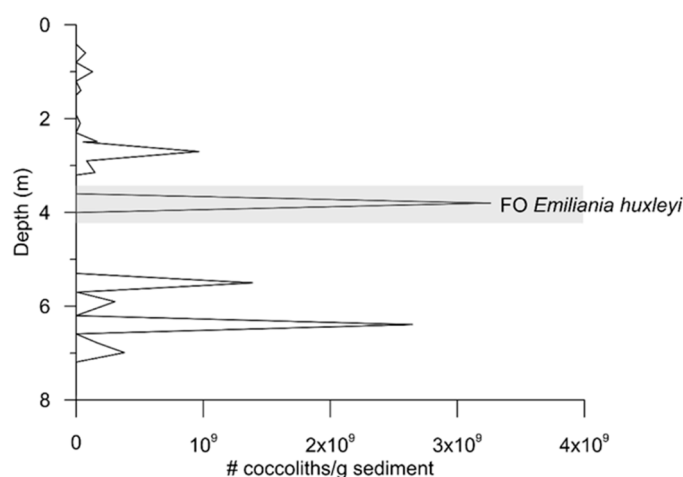


Figure 14. Absolute abundance of small *Gephyrocapsa* morphotypes from 0 to 8 mbsf. Gray highlighted area estimates an acme interval of the nannofossil. The secondary event coincides with the first occurrence of *Emiliana huxleyi*, which also lies within the gray area.

5. Conclusions

Twelve (12) calcareous nannofossil datums are documented in Pleistocene sediments of Site U1431D. This study is one of the first attempts to describe the distribution of *Gephyrocapsa* sp. 3 in SCS sediments and is suggested to be a well-defined marker for the subdivision of the Pleistocene in the marginal sea. The FO of *Gephyrocapsa* sp. 3 is near the reentrance event of medium *Gephyrocapsa* (reemG), which is also observed in several studies [7,21–23,60,81,83]. Nannofossil analysis suggests that the FO of large *Gephyrocapsa* (blG) is found above the LO of *Calcidiscus macintyreii*, which differs from shipboard results [43]. The LO of *Discoaster* species are determined using a semi-quantitative method to reduce the effect of reworking; however, the LO of *D. pentaradiatus* is very sporadic and therefore is not used as a marker for the Pleistocene in Site U1431D. The numerical ages of nannofossil datums are generated through correlation with magnetostratigraphy. The ages of the FO of *E. huxleyi* and LO of *P. lacunosa* are underestimated by 0.22 and 0.35 Ma, respectively, while bmG and LO of *C. macintyreii* are slightly overestimated by 0.12 and 0.15 Ma, respectively. The results of the magnetobiochronological calibration suggests further analysis using other stratigraphies (e.g., oxygen isotope stratigraphy, cyclostratigraphy).

Morphometric analysis of *Gephyrocapsa* coccoliths from the late Pliocene to Pleistocene sediments of Site U1431D allowed for the recognition and refinement of bioevents of the gephyrocapsids. These events are useful in updating the nannofossil biostratigraphy of the site. The events documented are the FO of medium *Gephyrocapsa* morphotypes (87.635 mbsf), the FO and LO of large *Gephyrocapsa* (78.985 and 60.65 mbsf, respectively), the reemG event (58.24 mbsf), and the FO and LO of *Gephyrocapsa* sp. 3 (57.605 and 25.925 mbsf, respectively). The trends of placolith length and bridge angles of *Gephyrocapsa* in Site U1431D are correlatable with previous studies on other ocean basins. The data

suggest that the change in the size of the geophyrocapsids points to an evolutionary trend rather than being caused by local or regional climate anomalies.

Supplementary Materials: The following are available online at <http://www.mdpi.com/2076-3263/10/10/388/s1>.

Author Contributions: Conceptualization, J.D.S.G. and A.M.P.-A.; methodology, J.D.S.G. and A.M.P.-A.; validation, J.D.S.G. and A.M.P.-A.; formal analysis, J.D.S.G.; investigation, J.D.S.G. and A.M.P.-A.; resources, A.M.P.-A.; data curation, J.D.S.G.; writing—original draft preparation, J.D.S.G.; writing—review and editing, J.D.S.G. and A.M.P.-A.; visualization, J.D.S.G.; supervision, A.M.P.-A.; project administration, A.M.P.-A.; funding acquisition, J.D.S.G. and A.M.P.-A. All authors have read and agreed to the published version of the manuscript.

Funding: This research was funded by the University of the Philippines Diliman, Office of the Vice Chancellor for Research and Development (OVCRD), grant number 171706 TSNE, and the University of the Philippines National Institute of Geological Sciences (UP NIGS) Research Grant for J.D.S.G.

Acknowledgments: The authors are thankful to the two anonymous reviewers whose reviews improved this paper. This research used samples and data provided by the International Ocean Discovery Program (IODP). The authors are grateful to the scientists and crew of IODP 349, UP NIGS and the Nannoworks Laboratory. J.D.S.G. gratefully acknowledges student assistants from the Institute for their invaluable help with sample processing.

Conflicts of Interest: The authors declare no conflict of interest. The funders had no role in the design of the study; in the collection, analyses, or interpretation of data; in the writing of the manuscript, or in the decision to publish the results.

Appendix A. Taxonomic Remarks

Calcidiscus leptoporus (Murray and Blackman, 1989) Loeblich and Tappan, 1978

Circular to subcircular proximal shield, birefringent. Distal shield non-birefringent with curved sutures. Shields easily separated. Closed central area.

REMARKS: Species is of little biostratigraphic value for the Pleistocene sediments of Site U1431D.

Calcidiscus macintyreii (Bukry and Bramlette, 1969a) Loeblich and Tappan, 1978

Circular proximal shield, birefringent. Distal shield non-birefringent with curved sutures, >10 μm with central opening.

Ceratolithus cristatus Kamptner, 1950

Strongly birefringent, c-axis lies in plane of horseshoe, perpendicular to length. Variable in size and degree of ornamentation.

REMARKS: Species is of little biostratigraphic value for the Pleistocene sediments of Site U1431D.

Ceratolithus telesmus Norris, 1965

Strongly birefringent, c-axis lies in plane of horseshoe, perpendicular to length. Long, sinuous arms.

REMARKS: Species is of little biostratigraphic value for the Pleistocene sediments of Site U1431D.

Coccolithus pelagicus (Wallich, 1877) Schiller, 1930

Elliptical placolith; central area open or with simple bar on the proximal surface.

REMARKS: Specimens of *Coccolithus pelagicus* with simple bar are only noted from section 10H and below (79.2 mbsf and below). The disappearance of *C. pelagicus* with bar may be a result of the migration of the species to higher latitudes within the Pleistocene. However, this event was not detected in the samples.

Cyclicargolithus floridanus (Roth and Hay in Hay et al., 1967) Bukry, 1971a [Coccolithus]

Coccoliths circular to sub-circular with small central area, <11 μm in width.

REMARKS: Occurs as reworked specimens.

Discoaster asymmetricus Gartner, 1969c

Asymmetric five-rayed variety of *D. brouweri*.

REMARKS: Occurs as reworked specimens.

Discoaster bellus Bukry and Percival, 1971

Five-rayed discoasters without any central knob or central area development. Straight rays that taper slightly and terminate in points. All rays lie on the same plane.

REMARKS: Occurs as reworked specimens.

Discoaster berggrenii Bukry, 1971b

Symmetric; five-rayed; rays curved; without bifurcations; well-developed central boss; central area 1-2x free ray length; adjacent rays separated at central-area.

REMARKS: Occurs as reworked specimens.

Discoaster blackstockae Bukry, 1973

four-rayed form with inter-ray angles of 60° and 120°. Considered a variant of *D. brouweri*.

REMARKS: Distribution within the core is very limited and does not parallel that of *D. brouweri*.

Discoaster brouweri Tan, 1927b emend. Bramlette and Riedel, 1954

Ray tips non-bifurcate but with marked proximal extensions giving it a distinctive concavo-convex form; six-rayed asterolith species.

Discoaster calcaris Gartner, 1967

Six-rayed asterolith, bifurcating asymmetrically at tip. Longer branch of bifurcation curved sharply proximally but extending only slightly laterally beyond tip of ray.

REMARKS: Occurs as reworked specimens.

Discoaster kugleri Martini and Bramlette, 1963

Central-area wide and flat; free rays short with notched ends rather than true bifurcations.

REMARKS: Occurs as reworked specimens.

Discoaster pentaradiatus Tan, 1927b

Five-rayed acute bifurcations; strongly concavo-convex and birefringent (each ray is a separate unit, with c-axes inclined slightly from vertical toward radial).

REMARKS: The distribution of *D. pentaradiatus* is sporadic in Site U1431D sediments, thus the LO of the species was not used for biostratigraphy.

Discoaster quinquerramus Gartner, 1969c

Five-rayed with concavo-convex rays. Central area with prominent distal sutural ridges and large proximal boss.

REMARKS: Occurs as reworked specimens.

Discoaster surculus Martini and Bramlette, 1963

Six-rayed and rarely with fewer rays with a stellate knob in the central area. From the knob, small ridges extend to the margin between the rays on one side of the asterolith and along the arms on the side. The slender rays are slightly enlarged at the end, and show a trifurcation, with the central spine extending beyond the arms.

Discoaster tamalis Kamptner, 1967

Concavo-convex rays. Calcite body consists of four arms arranged to form an orthogonal cross. There is no boss in the central area.

REMARKS: Occurs as reworked specimens.

Discoaster triradiatus Tan, 1927b

Symmetric three-rayed variety of *D. brouweri*.

Discoaster variabilis Martini and Bramlette, 1963

Central-area with proximal and distal ridges but weak bosses. Bifurcations well developed.

REMARKS: Occurs as reworked specimens.

Emiliania huxleyi (Lohmann, 1902) Hay and Mohler in Hay et al., 1967

No bridge, slits between distal shield elements.

Florisphaera profunda Okada and Honjo, 1973

Coccoliths formed of single angular 5-sided calcite units.

REMARKS: Species is of little biostratigraphic value for the Pleistocene sediments of Site U1431D.

Gephyrocapsa Kamptner, 1943

Like *Reticulofenestra* but with bridge formed from inner tube.

REMARKS: Size differences of coccoliths are used to separate the genus into different morphotypes for biostratigraphic purposes. The size criteria assigned by [21] is adopted in this study.

Gephyrocapsa sp. 3 Rio, 1982 (synonym: *G. parallela* Hay and Beaudry, 1973)

Large (4.0–6.4 μm) circular to sub-circular placolith, open central-area spanned by a bridge aligned 60°–90° to the long axis.

REMARKS: In this study, only those with a bridge aligned at 85°–90° to the long axis are considered as *Gephyrocapsa* sp. 3.

Helicosphaera carteri (Wallich, 1877) Kamptner, 1954

Medium to large size; flange ends in wing; two pores in central-area.

REMARKS: Species is of little biostratigraphic value for the Pleistocene sediments of Site U1431D.

Helicosphaera carteri var. *wallichi* (Lohmann, 1902) Theodoridis, 1984 [*H. wallichi*]

Like *H. carteri* but central-area with inclined pores.

REMARKS: Species is of little biostratigraphic value for the Pleistocene sediments of Site U1431D.

Helicosphaera inversa (Gartner, 1977 ex Gartner, 1980) Theodoridis, 1984

Like *H. carteri* but with large pores separated by prominent conjunct sub-horizontal bar usually with inverse direction.

REMARKS: Only one specimen of *H. inversa* is seen in Site U1431D samples; thus, it is not utilized for biostratigraphy.

Helicosphaera sellii (Bukry and Bramlette, 1969a) Jafar and Martini, 1975 [*Helicopontosphaera*]

Like *H. carteri* but pores large.

REMARKS: Distribution is sporadic in Site U1431D samples; thus, it is not utilized for biostratigraphy.

Neosphaera coccolithomorpha Lecal-Schaluder, 1950

Circular, ring-shaped coccoliths with open central-area. Single shield and tube, no distal shield. Superficially similar in light microscope to *Umbilicosphaera rotula* but shield paler in phase contrast and distinctive pseudoextinction cross seen in cross-polars at high focus.

REMARKS: Species is of little biostratigraphic value for the Pleistocene sediments of Site U1431D.

Pseudoemiliania lacunosa (Kamptner 1963) Gartner, 1969 [*Ellipsoplacolithus*]

Circular to broadly elliptical with variable number of slits in distal shield. Abundant in late Pliocene but well-developed, large circular forms occur only in the Pleistocene.

REMARKS: [84] observed that circular forms became much abundant during the late Pleistocene. However, circular forms are more abundant in the early Pleistocene in samples from Site U1431D.

Reticulofenestra minuta Roth, 1970

<3 µm which probably includes several different species.

REMARKS: Species is of little biostratigraphic value for the Pleistocene sediments of Site U1431D.

Reticulofenestra haqii Backman, 1978

3–5 µm which intergrades with *R. pseudoumbilicus*.

REMARKS: Species is of little biostratigraphic value for the Pleistocene sediments of Site U1431D.

Reticulofenestra pseudoumbilicus (Gartner, 1967b) Gartner, 1969c [*Coccolithus*]

>5 µm but for biostratigraphy it is better to separate the >7 µm specimens.

REMARKS: Occurs as reworked specimens.

Rhabdosphaera clavigera Murray and Blackman, 1898

Robust, club-shaped, 7–10 µm long.

REMARKS: Species is of little biostratigraphic value for the Pleistocene sediments of Site U1431D.

Scyphosphaera Lohmann, 1902

Vase-like coccoliths, generally large.

REMARKS: Species is of little biostratigraphic value.

Sphenolithus abies Deflandre in Deflandre and Fert, 1954

Similar to *S. moriformis* but more elevated and with cusped outline.

REMARKS: Occurs as reworked specimens.

Sphenolithus moriformis (Brönnimann and Stradner, 1960) Bramlette and Wilcoxon, 1967a (*Nannoturbella*)

Generalized form, no spine, upper and lower parts of similar size.

REMARKS: Occurs as reworked specimens.

Syracosphaera histrica Kamptner, 1941

Oblong or irregularly elliptical with bright rim and central-area.

REMARKS: Species is of little biostratigraphic value for the Pleistocene sediments of Site U1431D.

Umbellosphaera tenuis (Kamptner, 1937) Paasche in Markali and Paasche, 1955 [*Coccolithus*]

Trumpet-shaped coccoliths, with ridges on the distal surface

REMARKS: Species is of little biostratigraphic value for the Pleistocene sediments of Site U1431D.

Umbilicosphaera sibogae var. *sibogae* (Weber-van Bosse, 1901) Gaarder, 1970 [*Coccosphaera*]

Central opening wide, proximal shield monocyclic, wider than the distal shield.

REMARKS: Species is of little biostratigraphic value for the Pleistocene sediments of Site U1431D.

References

1. Shackleton, N.J.; Berger, A.; Peltier, W.R. An alternative astronomical calibration of the lower Pleistocene timescale based on ODP Site 677. *Trans. R. Soc. Edinb. Earth Sci.* **1990**, *81*, 251–261. [[CrossRef](#)]
2. Lisiecki, L.E.; Raymo, M.E. A Pliocene-Pleistocene stack of 57 globally distributed benthic $\delta^{18}\text{O}$ records. *Paleoceanography* **2005**, *20*, 1–17. [[CrossRef](#)]
3. de Boer, B.; Lourens, L.J.; van de Wal, R.S.W. Persistent 400,000-year variability of Antarctic ice volume and the carbon cycle is revealed throughout the Plio-Pleistocene. *Nat. Commun.* **2014**, *5*, 2999. [[CrossRef](#)] [[PubMed](#)]
4. Loutre, M.F.; Berger, A. Marine Isotope Stage 11 as an analogue for the present interglacial. *Glob. Planet. Chang.* **2003**, *36*, 209–217. [[CrossRef](#)]
5. Dickson, A.J.; Beer, C.J.; Dempsey, C.; Maslin, M.A.; Bendle, J.A.; McClymont, E.L.; Pancost, R.D. Oceanic forcing of the Marine Isotope Stage 11 interglacial. *Nat. Geosci.* **2009**, *2*, 428–433. [[CrossRef](#)]

6. Bown, P.R.; Young, J.R. Introduction. In *Calcareous Nannofossil Biostratigraphy*; British Micropalaeontological Society Publication Series; Chapman and Hall (Kluwer Academic Publishers): London, UK, 1998; pp. 1–15.
7. Raffi, I.; Backman, J.; Fornaciari, E.; Pälike, H.; Rio, D.; Lourens, L.; Hilgen, F. A review of calcareous nannofossil astrobiochronology encompassing the past 25 million years. *Quat. Sci. Rev.* **2006**, *25*, 3113–3137. [[CrossRef](#)]
8. Backman, J.; Raffi, I.; Rio, D.; Fornaciari, E.; Pälike, H. Biozonation and biochronology of Miocene through Pleistocene calcareous nannofossils from low and middle latitudes. *Newsl. Stratigr.* **2012**, *45*, 221–244. [[CrossRef](#)]
9. Gradstein, F.; Ogg, J.; Schmitz, M.; Ogg, G. *The Geologic Time Scale 2012*, 1st ed.; Elsevier BV: Amsterdam, The Netherlands, 2012.
10. Chepstow-Lusty, A.; Backman, J.; Shackleton, N.J. Comparison of upper Pliocene *Discoaster* abundance variations from North Atlantic sites 552, 607, 658, 659, 662; further evidence for marine plankton responding to orbital forcing. *Proc. Ocean. Drill. Program. Sci. Results* **1989**, *108*, 121–141.
11. Chepstow-Lusty, A.; Backman, J.; Shackleton, N.J. Palaeoclimatic control of upper Pliocene *Discoaster* assemblages in the North Atlantic. *J. Micropalaeontol.* **1991**, *9*, 133–143. [[CrossRef](#)]
12. Chepstow-Lusty, A.J.; Chapman, M.R. The decline and extinction of Upper Pliocene Discoasters: A comparison of two equatorial Pacific Ocean records. *J. Nannoplankton Res.* **1995**, *17*, 15–19.
13. Chapman, M.R.; Chepstow-Lusty, A.J. Late Pliocene climatic change and the global extinction of the discoasters: An independent assessment using oxygen isotope records. *Palaeogeogr. Palaeoclimatol. Palaeoecol.* **1997**, *134*, 109–125. [[CrossRef](#)]
14. Tangunan, D.N.; Baumann, K.-H.; Just, J.; LeVay, L.J.; Barker, S.; Brentegani, L.; De Vleeschouwer, D.; Hall, I.R.; Hemming, S.; Norris, R. The last 1 million years of the extinct genus *Discoaster*: Plio–Pleistocene environment and productivity at Site U1476 (Mozambique Channel). *Palaeogeogr. Palaeoclimatol. Palaeoecol.* **2018**, *505*, 187–197. [[CrossRef](#)]
15. Gartner, S. Late Pleistocene calcareous nannofossils in the caribbean and their interoceanic correlation. *Palaeogeogr. Palaeoclimatol. Palaeoecol.* **1972**, *12*, 169–191. [[CrossRef](#)]
16. Gartner, S. Calcareous nannofossil biostratigraphy and revised zonation of the Pleistocene. *Mar. Micropaleontol.* **1977**, *2*, 1–25. [[CrossRef](#)]
17. Thierstein, H.R.; Geitzenauer, K.R.; Molino, B.; Shackleton, N.J. Global synchronicity of late Quaternary coccolith datum levels: Validation by oxygen isotopes. *Geology* **1977**, *6*, 400–404. [[CrossRef](#)]
18. Samtleben, C. Die evolution der Coccolithophoriden-gattung *Gephyrocapsa* nach befunden im Atlantik. *Paläontol. Z.* **1980**, *54*, 91–127. [[CrossRef](#)]
19. Rio, D. The fossil distribution of coccolithophore genus *Gephyrocapsa* Kamptner and related Plio-Pleistocene chronostratigraphic problems. *Initial Rep. Deep Sea Drill. Proj.* **1982**, *68*, 325–343.
20. Rio, D.; Raffi, I.; Villa, G. Pliocene-Pleistocene calcareous nannofossil distribution patterns in the western Mediterranean. *Proc. Ocean. Drill. Program. Sci. Results* **1990**, *107*, 513–533.
21. Raffi, I.; Backman, J.; Rio, D.; Shackleton, N.J. Plio-Pleistocene nannofossil biostratigraphy and calibration to oxygen isotope stratigraphies from Deep Sea Drilling Project Site 607 and Ocean Drilling Program Site 677. *Paleoceanography* **1993**, *8*, 387–408. [[CrossRef](#)]
22. Wei, W. Calibration of Upper Pliocene-Lower Pleistocene nannofossil events with oxygen isotope stratigraphy. *Paleoceanography* **1993**, *8*, 85–99. [[CrossRef](#)]
23. Matsuoka, H.; Okada, H. Quantitative analysis of Quaternary nannoplankton in the subtropical northwestern Pacific Ocean. *Mar. Micropaleontol.* **1989**, *14*, 97–118. [[CrossRef](#)]
24. Matsuoka, H.; Okada, H. Time-progressive morphometric changes of the genus *Gephyrocapsa* in the Quaternary sequence of the tropical Indian Ocean, Site 709. *Proc. Ocean Drill. Program. Sci. Results* **1990**, *115*, 255–270.
25. Wei, K.-Y.; Yang, T.-N.; Huang, C.-Y. Glacial-Holocene calcareous nannofossils and paleoceanography in the northern South China Sea. *Mar. Micropaleontol.* **1997**, *32*, 95–114. [[CrossRef](#)]
26. Jian, Z.; Wang, L.; Kienast, M.; Sarnthein, M.; Kuhnt, W.; Lin, H.; Wang, P. Benthic foraminiferal paleoceanography of the South China Sea over the last 40,000 years. *Mar. Geol.* **1999**, *156*, 159–186. [[CrossRef](#)]
27. Wang, P. Response of Western Pacific marginal seas to glacial cycles: Paleoceanographic and sedimentological features. *Mar. Geol.* **1999**, *156*, 5–39. [[CrossRef](#)]

28. Nathan, S.A.; Leckie, R.M. Miocene planktonic foraminiferal biostratigraphy of Sites 1143 and 1146, ODP Leg 184, South China Sea. *Proc. Ocean Drill. Program. Sci. Results* **2003**, *184*, 1–43.
29. Li, B.; Jian, Z.; Li, Q.; Tian, J.; Wang, P. Paleooceanography of the South China Sea since the middle Miocene: Evidence from planktonic foraminifera. *Mar. Micropaleontol.* **2005**, *54*, 49–62. [[CrossRef](#)]
30. Su, X.; Liu, C.; Beaufort, L.; Tian, J.; Huang, E. Late Quaternary coccolith records in the South China Sea and East Asian monsoon dynamics. *Glob. Planet. Chang.* **2013**, *111*, 88–96. [[CrossRef](#)]
31. Lüdmann, T.; Kin Wong, H.; Wang, P. Plio–Quaternary sedimentation processes and neotectonics of the northern continental margin of the South China Sea. *Mar. Geol.* **2001**, *172*, 331–358. [[CrossRef](#)]
32. Liu, Z.; Colin, C.; Huang, W.; Le, K.P.; Tong, S.; Chen, Z.; Trentesaux, A. Climatic and tectonic controls on weathering in south China and Indochina Peninsula: Clay mineralogical and geochemical investigations from the Pearl, Red, and Mekong drainage basins. *Geochem. Geophys. Geosyst.* **2007**, *8*, 1–18. [[CrossRef](#)]
33. Wan, S.; Li, A.; Clift, P.D.; Stuut, J.-B.W. Development of the East Asian monsoon: Mineralogical and sedimentologic records in the northern South China Sea since 20 Ma. *Palaeogeogr. Palaeoclimatol. Palaeoecol.* **2007**, *254*, 561–582. [[CrossRef](#)]
34. Zong, Y.; Huang, G.; Li, X.Y.; Sun, Y.Y. Late Quaternary tectonics, sea-level change and lithostratigraphy along the northern coast of the South China Sea. In *River-Dominated Shelf Sediments of East Asian Seas*; Clift, P.D., Harff, J., Wu, J., Yan, Q., Eds.; Geological Society, Special Publications: London, UK, 2015; pp. 123–136.
35. Wang, P.; Li, Q.; Tian, J.; Jian, Z.; Liu, C.; Li, L.; Ma, W. Long-term cycles in the carbon reservoir of the Quaternary ocean: A perspective from the South China Sea. *Natl. Sci. Rev.* **2014**, *1*, 119–143. [[CrossRef](#)]
36. Cheng, X. Calcareous nannofossils in surface sediments of the central and northern parts of the South China Sea. *J. Micropalaeontol.* **1992**, *11*, 167–176. [[CrossRef](#)]
37. Cheng, X.; Wang, P. Controlling factors of coccolith distribution in surface sediments of the China seas: Marginal sea nannofossil assemblages revisited. *Mar. Micropaleontol.* **1997**, *32*, 155–172. [[CrossRef](#)]
38. Fernando, A.G.S.; Peleo-Alampay, A.M.; Lucero, E.S.; Wiesner, M.G. Surface sediment distribution of *Florisphaera profunda* in the South China Sea: An effect of dissolution? *J. Nannoplankton Res.* **2007**, *29*, 102–107.
39. Fernando, A.G.S.; Peleo-Alampay, A.M.; Wiesner, M.G. Calcareous nannofossils in surface sediments of the eastern and western South China Sea. *Mar. Micropaleontol.* **2007**, *66*, 1–26. [[CrossRef](#)]
40. Weiwu, D.; Yongyang, H. Tertiary calcareous nannofossil biostratigraphy in the north part of the South China Sea. *Acta Geol. Sin. Engl. Ed.* **1991**, *4*, 321–339. [[CrossRef](#)]
41. Huang, L. Calcareous nannofossil biostratigraphy in the Pearl River Mouth Basin, South China Sea, and Neogene reticulofenestrid coccoliths size distribution pattern. *Mar. Micropaleontol.* **1997**, *32*, 31–57. [[CrossRef](#)]
42. Su, X.; Xu, Y.; Tu, Q. Early Oligocene–Pleistocene calcareous nannofossil biostratigraphy of the northern South China Sea (Leg 184, Sites 1146–1148). In *Proceedings of the Ocean Drilling Program: Scientific Results*; Prell, W.L., Wang, P., Blum, P., Rea, D.K., Clemens, S.C., Eds.; Texas A&M University: College Station, TX, USA, 2004; Volume 184, pp. 1–24. ISBN 08845891.
43. Li, C.; Lin, J.; Kulhanek, D.K.; Williams, T.; Bao, R.; Briaies, A.; Brown, E.A.; Yifeng, C.; Clift, P.D.; Colwell, F.S.; et al. Site U1431. *Proc. Int. Ocean. Discov. Program.* **2014**, *349*, 1–54.
44. Li, C.-F.; Lin, J.; Kulhanek, D.K. South China Sea tectonics; opening of the South China Sea and its implications for southeast Asian tectonics, climates, and deep mantle processes since the late Mesozoic. In *International Ocean Discovery Program Expedition 349 Scientific Prospectus*; IODP Management International: College Station, TX, USA, 2013.
45. Xie, S.-P.; Xie, Q.; Wang, D.; Liu, W.T. Summer upwelling in the South China Sea and its role in regional climate variations. *J. Geophys. Res. Ocean.* **2003**, *108*. [[CrossRef](#)]
46. *The South China Sea: Paleooceanography and Sedimentology*; Wang, P.; Li, Q. (Eds.) Developments in Paleoenvironmental Research; Springer: Dordrecht, The Netherlands, 2009; Volume 13, ISBN 978-1-4020-9744-7.
47. Bown, P.R.; Young, J.R. Techniques. In *Calcareous Nannofossil Biostratigraphy*; British Micropalaeontological Society Publication Series; Chapman and Hall (Kluwer Academic Publishers): London, UK, 1998; pp. 16–28.
48. Perch-Nielsen, K. Cenozoic calcareous nannofossils. In *Plankton Stratigraphy*; Bolli, H.M., Saunders, J.M., Perch-Nielsen, K., Eds.; Cambridge University Press: Cambridge, UK, 1985; pp. 427–554.
49. Aubry, M.-P. *Handbook of Cenozoic Calcareous Nannoplankton, Book 1: Ortholithae (Discoasters)*; American Museum of Natural History; Micropaleontology Press: Flushing, NY, USA, 1984.

50. Aubry, M.-P. *Handbook of Cenozoic Calcareous Nannoplankton, Book 4: Heliolithae (Helicoliths, Cribriliths, Lopadoliths and Others)*; American Museum of Natural History; Micropaleontology Press: Flushing, NY, USA, 1990.
51. Backman, J.; Shackleton, N.J. Quantitative biochronology of Pliocene and early Pleistocene calcareous nannofossils from the Atlantic, Indian and Pacific oceans. *Mar. Micropaleontol.* **1983**, *8*, 141–170. [[CrossRef](#)]
52. Bollmann, J. Morphology and biogeography of *Gephyrocapsa* coccoliths in Holocene sediments. *Mar. Micropaleontol.* **1997**, *29*, 319–350. [[CrossRef](#)]
53. Liu, L.; Maiorano, P.; Zhao, X. Pliocene-Pleistocene calcareous nannofossils from the Iberia abyssal plain. *Proc. Ocean Drill. Program. Sci. Results* **1996**, *149*, 147–164.
54. Marino, M.; Maiorano, P.; Monechif, S. Quantitative Pleistocene calcareous nannofossil biostratigraphy of Leg 86, Site 577 (Shatsky Rise, NW Pacific Ocean). *J. Nannoplankton Res.* **2003**, *25*, 25–37.
55. Houghton, S.D. Late Neogene calcareous nannofossil biostratigraphy and paleoceanography of ODP Hole 677A, Panama Basin. *Proc. Ocean. Drill. Program. Sci. Results* **1989**, *111*, 277–285.
56. Raffi, I.; Flores, J.-A. Pleistocene through Miocene calcareous nannofossils from eastern Equatorial Pacific Ocean (Leg 138). *Proc. Ocean. Drill. Program. Sci. Results* **1995**, *138*, 233–282.
57. Kameo, K.; Bralower, T.J. Neogene calcareous nannofossil biostratigraphy of sites 998, 999, and 1000, Caribbean Sea. *Proc. Ocean. Drill. Program. Sci. Results* **2000**, *165*, 3–17.
58. Curry, W.B.; Shackleton, N.J.; Richter, C.; Backman, J.E.; Bassinot, F.; Bickert, T.; Chaisson, W.P.; Cullen, J.L.; deMenocal, P.; Dobson, D.M.; et al. Site 925. *Proc. Ocean. Drill. Program. Part. Initial Rep.* **1995**, *154*, 55–152.
59. Lupi, C.; Bordiga, M.; Cobianchi, M. *Gephyrocapsa* occurrence during the Middle Pleistocene transition in the Northern Pacific Ocean (Shatsky Rise). *Geobios* **2012**, *45*, 209–217. [[CrossRef](#)]
60. de Kaenel, E.P.; Siesser, W.G.; Murat, A. Pleistocene calcareous nannofossil biostratigraphy and the western Mediterranean sapropels, sites 974 to 977 and 979. *Proc. Ocean. Drill. Program. Sci. Results* **1999**, *161*, 159–183.
61. Lourens, L.J.; Hilgen, F.J.; Shackleton, N.J.; Laskar, J.; Wilson, D. The Neogene Period. In *A Geologic Time Scale 2004*; Gradstein, F., Ogg, J., Smith, A., Eds.; Cambridge University Press: New York, NY, USA, 2004; pp. 409–440.
62. Roberts, D.G.; Schnitker, D.; Baldauf, J.G.; Desprairies, A.; Homrighausen, R.; Huddleston, P.F.; Kaltenback, A.J.; Krumsiek, K.A.O.; Morton, A.C.; Murray, J.W.; et al. Sites 552–553. *Initial Rep. Deep Sea Drill. Proj.* **1984**, *81*, 31.
63. Ruddiman, W.F.; Kidd, R.B.; Baldauf, J.G.; Clement, B.M.; Dolan, J.F.; Eggers, M.R.; Hill, P.R.; Keigwin, L.D., Jr.; Mitchell, M.; Philipps, I.; et al. Site 607. *Initial Rep. Deep Sea Drill. Proj.* **1987**, *94*, 75.
64. Sprovieri, R.; Di Stefano, E.; Howell, M.; Sakamoto, T.; Di Stefano, A.; Marino, M. Integrated calcareous plankton biostratigraphy and cyclostratigraphy at Site 964. *Proc. Ocean. Drill. Program. Sci. Results* **1998**, *160*, 155–166.
65. Kameo, K.; Okada, M. Calcareous nannofossil biochronology from the upper Pliocene to lower Pleistocene in the southernmost Boso Peninsula, central part of the Pacific side of Japan. *J. Asian Earth Sci.* **2016**, *129*, 142–151. [[CrossRef](#)]
66. Wu, H.; Zhao, X.; Shi, M.; Zhang, S.; Li, H.; Yang, T. A 23 Myr magnetostratigraphic time framework for Site 1148, ODP Leg 184 in South China Sea and its geological implications. *Mar. Pet. Geol.* **2014**, *58*, 749–759. [[CrossRef](#)]
67. Shyu, J.-P.; Merrill, D.L.; Hsü, V.; Kaminski, M.A.; Müller, C.M.; Nederbragt, A.J.; Scherer, R.P.; Shibuya, H. Biostratigraphic and magnetostratigraphic synthesis of the Celebes and Sulu Seas, Leg 124. *Proc. Ocean. Drill. Program. Sci. Results* **1991**, *124*, 11–35.
68. Mayer, L.A.; Pisias, N.G.; Janecek, T.R.; Baldauf, J.G.; Bloomer, S.F.; Dadey, K.A.; Emeis, K.-C.; Farrell, J.; Flores, J.A.; Galimov, E.M.; et al. Site 846. *Proc. Ocean. Drill. Program. Part. Initial Rep.* **1991**, *138*, 265.
69. Backman, J.; Duncan, R.A.; Peterson, L.C.; Baker, P.A.; Baxter, A.N.; Boersma, A.; Cullen, J.L.; Droxler, A.W.; Fisk, M.R.; Greenough, J.D.; et al. Site 710. *Proc. Ocean. Drill. Program. Part. Initial Rep.* **1988**, *115*, 589.
70. Barton, C.E.; Bloemendal, J. Paleomagnetism of sediments collected during Leg 90, southwest Pacific (DSDP). In *Initial Reports of Deep Sea Drilling Program*; Texas A & M University, Ocean Drilling Program: College Station, TX, USA, 1986; Volume 90, pp. 1273–1316.

71. Lohman, W.H. Calcareous nannoplankton biostratigraphy of the southern Coral Sea, Tasman Sea, and southwestern Pacific Ocean, Deep Sea Drilling Project Leg 90: Neogene and Quaternary. In *Initial Reports of the Deep Sea Drilling Project*; Texas A & M University, Ocean Drilling Program: College Station, TX, USA, 1986; Volume 90.
72. Bickert, T.; Curry, W.B.; Wefer, G. Late Pliocene to Holocene (2.6–0 Ma) western Equatorial Atlantic deep-water circulation; inferences from benthic stable isotopes. *Proc. Ocean. Drill. Program. Sci. Results* **1997**, *154*, 239–254.
73. Takayama, T.; Sato, T. Coccolith biostratigraphy of the North Atlantic Ocean, Deep Sea Drilling Project Leg 94. *Initial Rep. Deep Sea Drill. Proj.* **1987**, *94*, 651–702.
74. Martini, E. *Standard Tertiary and Quaternary Calcareous Nannoplankton Zonation*; Farinacci, A., Ed.; Tecnoscienza: Rome, Italy, 1971; pp. 739–785.
75. Muza, J.P. Calcareous nanofossil biostratigraphy from the Japan Sea, sites 798 and 799; evidence for an oscillating Pleistocene oceanographic frontal boundary. *Proc. Ocean. Drill. Program. Sci. Results* **1992**, *127*, 155–169.
76. Castradori, D. Calcareous nanofossil biostratigraphy and biochronology in Eastern Mediterranean deep-sea cores. *Riv. Ital. Paleontol. E Stratigr.* **1993**, *99*, 107–126.
77. Maiorano, P.; Marino, M. Calcareous nanofossil bioevents and environmental control on temporal and spatial patterns at the early–middle Pleistocene. *Mar. Micropaleontol.* **2004**, *53*, 405–422. [[CrossRef](#)]
78. Geitzenauer, K. The Pleistocene calcareous nannoplankton of the subantarctic Pacific Ocean. *Deep Sea Res.* **1972**, *19*, 45–60. [[CrossRef](#)]
79. Di Stefano, E.; Caracausi, S.; Incarbona, A.; Velardi, S. Size variations in the genus *Gephyrocapsa* during the Early Pleistocene in the eastern Mediterranean. *Ital. J. Geosci.* **2014**, *133*, 474–480. [[CrossRef](#)]
80. McIntyre, A.; Bé, A.W.H.; Roche, M.B. Modern Pacific Coccolithophorida: A paleontological thermometer. *Trans. N. Y. Acad. Sci.* **1970**, *32*, 720–731. [[CrossRef](#)]
81. Raffi, I. Revision of the early-middle Pleistocene calcareous nanofossil biochronology (1.75–0.85 Ma). *Mar. Micropaleontol.* **2020**, *45*, 25–55. [[CrossRef](#)]
82. Maiorano, P.; Marino, M.; Di Stefano, E.; Ciaranfi, N. Calcareous nanofossil events in the Lower-Middle Pleistocene transition at the Montalbano Jonico section and ODP site 964: Calibration with isotope and sapropel stratigraphy. *Riv. Ital. Paleontol. E Stratigr.* **2004**, *110*, 547–557.
83. Marino, M.; Maiorano, P.; Flower, B.P. Calcareous nanofossil changes during the Mid-Pleistocene Revolution: Paleoeologic and paleoceanographic evidence from North Atlantic Site 980/981. *Palaeogeogr. Palaeoclimatol. Palaeoecol.* **2011**, *306*, 58–69. [[CrossRef](#)]
84. Hay, W.W. Calcareous nanofossils from cores recovered on Leg 4. *Initial Rep. Deep Sea Drill. Proj.* **1970**, *4*, 455–501.
85. Hine, N.; Weaver, P.P.E. Quaternary. In *Calcareous Nannofossil Biostratigraphy*; British Micropalaeontological Society Publication Series; Chapman and Hall (Kluwer Academic Publishers): London, UK, 1998; pp. 266–283.
86. Young, J.R. A Quaternary nanofossil range chart. *Int. Nannoplankton Assoc. Newsl.* **1991**, *13*, 14–17.

